Titre: Title:	Three-Dimensional Printing of Multifunctional Nanocomposites: Manufacturing Techniques and Applications
Auteurs: Authors:	Rouhollah D. Farahani, Martine Dubé et Daniel Therriault
Date:	2016
Type:	Article de revue / Journal article
Référence: Citation:	Farahani, R. D., Dubé, M. & Therriault, D. (2016). Three-Dimensional Printing of Multifunctional Nanocomposites: Manufacturing Techniques and Applications. *Advanced Materials*, *28*(28), p. 5794-5821. doi:10.1002/adma.201506215

Document en libre accès dans PolyPublie
Open Access document in PolyPublie

URL de PolyPublie: PolyPublie URL:	https://publications.polymtl.ca/10415/
Version:	Version finale avant publication / Accepted version Révisé par les pairs / Refereed
Conditions d'utilisation: Terms of Use:	Tous droits réservés / All rights reserved

Document publié chez l'éditeur officiel
Document issued by the official publisher

Titre de la revue: Journal Title:	Advanced Materials (vol. 28, no 28)
Maison d'édition: Publisher:	Wiley
URL officiel: Official URL:	https://doi.org/10.1002/adma.201506215
Mention légale: Legal notice:	"This is the peer reviewed version of the following article: Farahani, R. D., Dubé, M. & Therriault, D. (2016). Three-Dimensional Printing of Multifunctional Nanocomposites: Manufacturing Techniques and Applications. *Advanced Materials*, *28*(28), p. 5794-5821, which has been published in final form at https://doi.org/10.1002/adma.201506215. This article may be used for non-commercial purposes in accordance with Wiley Terms and Conditions for Use of Self-Archived Versions. This article may not be enhanced, enriched or otherwise transformed into a derivative work, without express permission from Wiley or by statutory rights under applicable legislation. Copyright notices must not be removed, obscured or modified. The article must be linked to Wiley's version of record on Wiley Online Library and any embedding, framing or otherwise making available the article or pages thereof by third parties from platforms, services and websites other than Wiley Online Library must be prohibited."

Three-Dimensional Printing of Multifunctional Nanocomposites: Manufacturing Techniques and Applications

By *Dr. R.D. Farahani*[*], *Prof. M. Dubé*, and *Prof. D. Therriault*

[*] Dr. R. D. F Corresponding-Author, Prof. M. D. Author-Two
École de technologie supérieure, Department of Mechanical Engineering, Montréal, CANADA H3C 1K3,
E-mail: rouhollah.farahani@polymtl.ca
Prof. D.T. Author-Three
Laboratory for Multiscale Mechanics (LM^2), Department of Mechanical Engineering, École Polytechnique de Montréal, C.P. 6079, Succ. Centre-ville, Montréal, CANADA H3C 3A7.

Abstract

The integration of nanotechnology into three-dimensional printing (3DP) offers huge potentials and opportunities for the manufacturing of 3D engineered materials exhibiting optimized properties and multifunctionality. The purpose of this paper is to review the literature related to different 3DP techniques used to fabricate 3D structures at the macro- and microscale made of nanocomposite materials. The current state of the art fabrication methods, their main characteristics (e.g., resolutions, advantages, limitations), the process parameters and materials requirements are discussed. A comprehensive review is carried out on the use of metal and carbon-based nanomaterials incorporated into polymers or hydrogels for the manufacturing of 3D structures, mostly at the microscale, using different 3D printing techniques. Several methods including but not limited to microstereolithography, extrusion-based direct write technologies, inkjet printing techniques and popular powder bed technology are discussed. Various examples of 3D nanocomposite macro- and microstructures
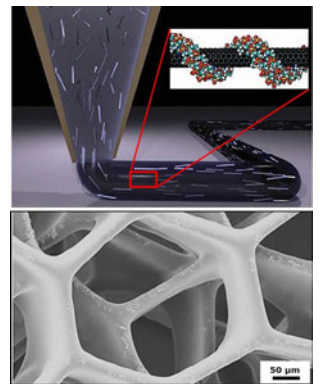
manufactured using different 3D printing technologies for a wide range of domains such as MEMS, lab-on-a-chip, microfluidics, engineered materials and composites, microelectronics, tissue engineering and biosystems are reviewed. The parallel advances on materials and techniques are still required in order to employ the full potential of 3D printing of multifunctional nanocomposites.

1. Introduction

Three-dimensional (3D) printing has drawn tremendous attention from both academia and industry with its potential applications in various fields such as aerospace, automotive, medical and pharmaceutical domains. 3D printing (3DP) represents a family of flexible manufacturing techniques that enables fast and accurate fabrication of structures with complex 3D features and a broad range of size from submicron to several meters.[1, 2] There are numerous benefits offered by this technology such as the ease of use, reliability, cost-effectiveness, and diversity of the compatible materials (e.g., metals, polymers and ceramics). These characteristics enable making structures for a wide variety of applications ranging from microelectronics and micro-systems (e.g., sensors and lab-on-chips) to aerospace structures such as aircraft engine bracket and fuel nozzles.[2] Many 3DP techniques enable building 3D miniaturized microsystems with smaller planar footprint compared to two-dimensional (2D) structures. Various complex 3D features including supported (i.e., layer-by-layer),[1, 3] self-supported[3] (e.g., spanning filament[4]) and 3D freeform[5, 6] structures can be fabricated using most of the 3DP techniques.

The combination of 3DP and nanotechnology opens new avenues for the manufacturing of 3D engineered materials exhibiting optimized properties and multifunctionality. For instance, the incorporation of nanomaterials (e.g., carbon nanotubes) into 3DP not only results in a better functionality of the manufactured device (e.g., electrical conductivity, electromechanical/chemical

sensitivity, mechanical strength), it may also improve printability (i.e., material requirements) of the feedstock materials for the 3DP processes. To benefit from the combination of nanotechnology and 3DP, it is essential to improve the current understanding of the various types of nanomaterials and nanocomposites and their processing, as well as finding the proper printing techniques to build 3D systems and engineered structures. Despite the many advantages offered by the union of nanotechnology and 3DP, several challenges (e.g., nanocomposite processing, cost, reliability) have to be addressed in order to employ the full potential of 3DP of multifunctional nanocomposites. For instance, the extrusion-based 3DP technique may encounter problems such as nanomaterials aggregation or the increase of viscosity after addition of nanoparticles to the printing materials that may cause nozzle clogging. Therefore, a proper mixing strategy has to be used in order to disperse nanofillers into the host material before 3D printing.

This review paper will mostly focus on 3DP techniques through which nanocomposite materials were used for the manufacturing of microstructured macro and micro-devices, taking into account the advantages and limitations for materials and techniques. To this end, several 3DP techniques have emerged to fabricate 2D and 3D microstructures such as photolithography techniques,[7] fused deposition modeling,[8] powder bed technology and several new-emerging direct-write techniques.[9, 10] Thus far, the research on this topic has been conducted based on two major approaches: 1. discontinuous printing of the host (i.e., unfilled) material and the addition of nanomaterials at the desired time or layer during the fabrication, and, 2. printing of a pre-mixed material composed of the nanomaterials and the matrix (resin or solution). This review paper will mainly focus on the works which are based on the second approach; however the first approach will be touched by mentioning a few interesting works. Therefore, the paper is organized as follows: first, different aspects related to nanocomposites including their mixing strategies, properties and benefits over typical printing materials (e.g., pure resins) are briefly mentioned. Printing of

nanocomposite materials in 2D or thin 3D, the techniques and their limitations/difficulties are then presented. This is then followed by the introduction of several 3DP techniques which are capable of manufacturing 3D structures. The applications of nanocomposite-based microstructures in different fields such as MEMS, lab-on-a-chip systems, microelectronics and tissue engineering are also discussed in detail. Finally, several interesting recent works in which nanomaterial solutions (instead of polymer nanocomposites) have been used as printing materials are briefly presented. The main outcomes of this review are to show the huge potential in combining nanotechnology and 3DP and also to guide the reader in finding the most suitable 3DP technique for the fabrication of 2D and 3D microstructures with the desired geometry for a targeted application. The interested readers could find additional information regarding the suppliers/manufacturers of the main equipment that have been used in the 3DP techniques mentioned in this review as **Table S1** in "Supplementary information".

2. Nanocomposites: preparation strategies, properties and benefits

3DP approach has traditionally been used for rapid prototyping of a structure before production. Recently, it has been a growing interest and progress toward the use of 3DP for manufacturing of structures and devices.[11-13] To this end, 3DP materials that provide functionality beyond the conventional pure printing materials (e.g., pure resins) are required to meet the property requirements for the fabricated structures for targeted applications. Nanomaterials can confer multifunctional properties to the printing pure materials where they can serve as structural,[14-16] sensing,[12, 17, 18] heating,[19] magnetic[20] and conductive elements.[21, 22] The resulting nanocomposites possessing unique properties could expand the utilization of 3DP in various areas. Different types of nanofillers such as carbonaceous nanofillers, nanoclay, and metallic nanofillers have been incorporated into a wide range of hydrogels and polymer matrices, both thermoplastics

and thermosetting resins for manufacturing of structures with functionality and/or improved properties. For instance, due to their excellent conductivity, metallic nanofillers such as silver nanowires[23] and nanoparticles[24] as well as carbonaceous nanofillers such as carbon nanotubes,[25] carbon nanofibers,[26] and graphene[22, 27] are increasingly used as conductive nanofillers in insulating polymers to fabricate electrically conductive nanocomposites. Such nanocomposites have been used in a wide range of applications ranging from sensing devices (e.g., liquid sensor,[12] strain sensor[18]) to electromagnetic shielding protection for aerospace structures.[23, 28]

The performance (e.g., mechanical, thermal and electrical properties) of the final product is highly dependent on features such as nanofillers intrinsic characteristics, morphology (e.g., dispersion) of the nanocomposites and interfacial interaction between nanofillers and the host materials. To improve the mechanical properties, a few steps of chemical treatment that may involve purification and surface functionalization may be applied on the nanofillers before nanocomposite processing for all types of the host materials to achieve a better dispersion and higher nanofiller-matrix interfacial interaction. Surface treatment of nanofillers may improve both fillers dispersion and their adhesion to the matrix through functional groups, and thus, the mechanical properties of the nanocomposite.[29] Both non-covalent functionalization using surfactants (e.g., carboxymethylcellulose,[30] protoporphyrin[31, 32]) and also covalent functionalization through grafting functional groups such as carboxylic groups[33, 34] and epoxide groups[35] to nanofillers surface have been reported in the literature. In turn, the surface functionalization and high level of nanofiller dispersion may be avoided when maximum electrical conductivity is required.[36] In particular for high aspect ratio (i.e., length/diameter) fillers such as carbon nanotubes, the surface functionalization may destroy the wall integrity, break the nanofillers, and consequently reduce their aspect ratio.[37] Understanding the relationships among those parameters and the nanocomposite properties can therefore help in choosing a proper mixing

strategy and thus, the design of nanocomposite materials. A comprehensive study on the effect of nanofillers' surface modification on polymer nanocomposites properties has been reviewed by Rong et al.[38]

The nanocomposite processing strategy is usually dependent of the type of the matrix. The main processing methods may include either one or a combination of solution mixing, high shear mixing and in-situ polymerization. In case of thermosetting matrix, solution processing by stirring and/or sonication, shear mixing in a three-roll mill mixer and the combination of both are the most popular mixing strategies.[32, 33] Nanocomposite mixing in case of thermoplastics is usually carried out by using twin screw extruders or batch mixers (e.g., brabenders).[39] High shear forces and complicated flow in this type of equipment produce a nanocomposite with excellent nanofillers dispersion.[40] The solution processing can also be used for thermoplastics and hydrogels if they can be dissolved in a solvent.[41, 42]

There are numerous review articles that discussed different nanocomposite mixing strategies and the improvement of properties such as magnetic, mechanical, thermal and electrical.[14, 43] Following, a few interesting works that are related to the use of nanocomposites in 3DP are only presented. Yugang et al.[44] studied mechanical properties and viscosity of a photopolymer filled with TiO_2 nanoparticles for rapid prototyping. The nanofillers were first functionalized using a silane coupling agent (KH 570) to create hydroxyl groups on their surface. The addition of only 0.25 wt.% nanofillers led to increase of 89% of the tensile strength, 18% of the modulus, and 6% of the flexural strength of the nanocomposite compared those of the pure resin. The viscosity of the nanocomposites containing functionalized nanofillers (hydroxyl groups) was higher than that of the nanocomposite with pristine nanofillers, possibly due to increased filler-matrix interfacial interaction. Although the lower viscosity is preferred for some 3DP techniques such as stereolithography for the surface quality and fabrication accuracy, the higher filler-matrix

interaction, provided by the functional groups helped prevent the nanofillers precipitation. Goodridge *et al.*[45] investigated the effects of carbon nanofiber (CNF) addition on the processing parameters and mechanical properties of polyamide-12 (PA12) nanocomposite fabricated by laser sintering. The CNFs/PA12 nanocomposite powder was first prepared by melt mixing and cryogenic milling. The dynamic mechanical testing revealed an increase of 22% in the nanocomposite storage modulus compared to the pure material. Farahani *et al.*[16] studied the functionalization of purified single-walled carbon nanotubes (SWCNTs) using biomaterials and its effect on morphological, mechanical and electrical properties of the 3D printed nanocomposite filaments. The resin was a one-component dual cure (ultraviolet/heat curable) epoxy resin (UV15DC80, Master Bond Inc.). The nanocomposite was prepared by mixing the bio-functionalized SWCNTs (BF-SWCNTs) with the epoxy resin in a solution of dichloromethane by sonication in an ultrasonication bath, followed by high shear mixing in a three-roll mill mixer. The BF-SWCNTs were found to be capable of interacting with epoxy groups to facilitate the load transfer. The biofunctionalization also improved the nanotube dispersion into the epoxy matrix. Tensile mechanical characterization on the nanocomposites demonstrated 76% increase of strength and 93% increase of modulus with the addition of only 1 wt.% of BF-SWCNTs. The electrical measurements revealed an increase of electrical resistivity (by 129%) for the BF-SWCNTs nanocomposite in comparison to the nanocomposite containing solely purified SWCNTs. According to the authors, the electrical conductivity change might be attributed to the presence of insulating biomolecules surrounding the SWCNTs. These multifunctional nanocomposite materials might have potential for the fabrication of easily-manipulated biosensors. Lebel *et al.*[32] studied the effect of nanofillers (SWCNTs and fumed silica particles) on rheological and mechanical properties of 3D printed filaments. The mixing strategy used in their work involved a non-covalent functionalization of the SWCNTs by a surfactant (zinc protoporphyrin IX), sonication and three-roll mill shear mixing. The resin used was

a UV-curable acrylic-based resin (NEA 123MB, Norland Products Inc). Nanocomposite materials with different nanofillers concentrations and mixing strategies were then prepared for comparison purposes. The addition of 0.5 wt.% into the pure resin led to an increase of the viscosity and the appearance of a shear-thinning behavior. The further incorporation of 5 wt.% fumed silica nanoparticles significantly increased the viscosity of the nanocomposites and enabled printing of nanocomposite microfilaments. Mechanical characterization on the nanocomposite microfibers demonstrated significant enhancement in tensile modulus (~15 times) and strength (by 64%) compared to those containing 5 wt.% fumed silica (i.e., without SWCNTs). The authors believed that the non-covalent functionalization of SWCNTs and the selection of the proper mixing strategy including sonication and high shear mixing are not only responsible for such increase of mechanical properties, they also provided a better nanofiller dispersion and tailored the viscosity behavior of the nanocomposites for 3DP. Chizari *et al.*[46] developed highly conductive nanocomposite materials through mixing of polylactic acid (PLA) and carbon nanotubes using a ball milling machine (SPEX SamplePrep 8000M). This method enabled the fabrication of nanocomposites with a very high concentration of nanotubes (up to 40%). Dissolving the nanocomposites into DCM solvent (10-25 wt.% of nanocomposite in solution) tailored the viscosity of the resulting materials and, thus enabled the fabrication of microfilaments by extruding the materials through a micronozzle. The printed filaments with the diameter of ~70 μm showed a conductivity as high as 4000 S/m. According to the authors, this type of conductive materials has potentials for several applications such as electromagnetic interference (EMI) shielding, sensors, antistatic coatings and flexible electrodes. Several other examples showing the benefits of the nanocomposites will be discussed throughout the paper.

2. Printing of nanocomposite structures with planar or thin 3D features

This section deals with the methods based on the inkjet printing technique with the capability of printing nanocomposite microstructures with either planar or thin 3D features. Other techniques such as microcontact printing with the ability of nanocomposite planar printing also exist,[47, 48] but they are not within the scope of the present paper, thus are not discussed here. The inkjet printing consists in the deposition of small drops of ink materials using a jet onto a substrate. The inkjet printing is an inexpensive method with high throughput that has been used to fabricate devices for different application such as conductive metal wirings and strain gauges.[49] Thin 3D structures are fabricated when the printing is repeated to deposit ink droplets in layers. Continuous and drop-on-demand methods are the two main categories of the inkjet printing technique. **Fig. 1a** shows a schematic of a piezoelectric drop-on-demand inkjet printing technique. A drop with a calibrated velocity is ejected from a nozzle when the piezoelectric actuator expands to create a positive pressure upon the application of voltage.[50] **Fig. 1b** shows image of an ink droplet of silver nitrate solution in water and ethanol after being ejected from the nozzle. To make spherical droplets for an accurate fabrication in this technique, the jetting parameters (e.g., voltage, frequency and viscosity wave form) have to be properly set. Despite advances towards the deposition of drops at high resolution in the inkjet printing methods, the materials used are limited to inkjet printable and UV-curable ink materials.[51] **Fig. 1c** shows inkjet printed filaments of graphene oxide-filled polymer nanocomposites during electrical resistivity measurement.

Chiolerio *et al.*[49] studied the preparation of a novel conductive nanocomposite composed of silver precursors (AgSbF$_6$, 30 wt.%) and titanium (TiO$_2$, 5 wt.%) nanoparticles mixed with a photocurable resin (polyethylene glycol diacrylate containing 2 wt.% of radical photoinitiators). Using this type of nanocomposite materials, a high conductivity can be achieved upon reduction of silver precursors to silver nanoparticles in the presence of the titanium nanoparticles. The addition

of water (1:1 proportion to the resin) to the nanocomposite facilitated the dispersion of materials and made the solution suitable for the inkjet printing. The nanocomposite solution was then used to fabricate a strain sensor with a geometry similar to that of the metallic strain gauges as shown in the inset of **Fig. 1d**. The inkjet printing equipment was a Piezoelectric Jetlab 4 Printer (MicroFab Technologies Inc.) equipped with a MJ-AT-01 dispenser with a 60 μm nozzle. The fabricated sensor consisted of 6 layers (printed on top of each other) with a step size of 100 μm. The electromechanical measurements were performed on the fabricated sensors to assess their sensitivity in terms of gauge factor (GF) (**Fig. 1d**). The inkjet-printed strain gauge for the case of no-treatment (IjP in the figure) showed GF values as high as 220, which is two orders of magnitude higher than those of commercial metallic gauges. Additional treatments such as UV curing and metal sintering changed the conductivity regime and thus resulted in lower sensitivity.

Wang *et al*.[52] reported the inkjet printing of a conductive ink composed of annealed graphene sheets decorated with silver nanoparticles. The inkjet equipment was a Fujifilm Dimatix Materials Printer (DMP-2800) equipped with a 10 pL drop cartridge (DMC-11610). The nanocomposite films (15 printing layers) made of the silver nanoparticle-decorated graphene showed a conductivity of 2.16×10^3 S/m with high potential for applications such as in flexible electronic devices. Chi *et al*.[53] reported on the use of the inkjet printing for the fabrication of a flexible nanocomposite supercapacitor. The device was composed of a freestanding graphene paper supporting a 3D porous graphene hydrogel (GH) - polyaniline (PANI) nanocomposite. **Fig. 2** represents different aspects of the device. The hybrid nanocomposite capacitor exhibited excellent electrical conductivity and mechanical flexibility, and high cycling performance. While PANI is known as a highly promising electrode material to be used in supercapacitors, its electrical conductivity has to be tailored. The addition of the GH nanoparticles into PANI polymer improved its moderate electrical conductivity and enabled the fabrication of the nanohybrid supercapacitors. The device was fabricated using

graphene oxide and GH−PANI inks (concentration of 2 mgmL^{-1} in water, droplet size = 10 pL) by a commercial Dimatix Materials Printer (DMP 2800, Dimatix-Fujifilm Inc.).

Elliott *et al.*[54] studied the incorporation of quantum dots (QD) (0.5 wt.%) into a photopolymer (Object VeroClear) and its effect on rheology and jettability of the resulting nanocomposites. The QDs at this low loading did not affect the viscosity of the resin and kept it in the range of jettability. The equipment was an Objet PolyJet 3D printer having several inkjet nozzles with a diameter of ~60 μm and a resolution of 32 μm. This equipment enables the fabrication of structures in a layer-by-layer manner using an integrated UV light for photopolymerization of the deposited materials. The PolyJet printer allows the use of different materials at a time for the fabrication of multifunctional materials. The authors mentioned that this type of inkjet printed nanocomposite structures may find several applications such as LEDs, sensing, data storage, anti-counterfeiting or visual indicators of increased temperature.[54]

3. 3DP techniques

This section discusses several 3DP methods used for the fabrication of 3D nanocomposite-based structures. A few conventional methods as well as several newly developed 3DP techniques which are based on the extrusion of material filaments through fine nozzles are reviewed. It should be mentioned that all the 3DP methods discussed in the next sections are also capable of planar printing. The examples of planar or 3D thin microstructures fabricated by those techniques may be also provided.

3.1. Conventional 3DP techniques

3.1.1. Powder-bed technology as a binding-based inkjet printing

Powder-bed technology, shown schematically in **Fig. 3a**, is a 3DP technique which is based on inkjet printing. In this technique, a low viscosity liquid adhesive is printed over the surface of a powder bed and binds the adjacent powder particles, creating a desired 2D pattern. The powder bed is then lowered to a desired height and a new layer of the powder is spread over the surface of the first layer and the second layer is patterned by the inkjet printing of the liquid binding adhesive. The process is repeated until the desired layers are deposited and the remaining unbounded powder is finally removed. Metals, polymers and ceramics can be used in the powder bed technology.[55] Due to very low viscosity of the liquid adhesive, consistent droplets can be generated without nozzle clogging. However, the resolution of the printed structures using this technique is relatively low (e.g., minimum feature size of several hundred microns) due to spreading of the liquids into the powder bed.[56] The accuracy of the fabrication depends on many parameters such as adhesive-powder interaction, powder type, powder particle size, adhesive droplet size, its viscosity and velocity.[47] The fabrication speed of the powder bed technology is very fast, however, the part surface is usually rough. Compared to other 3DP methods, the powder bed technology is expensive (0.05 – 2 M$). To the best of our knowledge, the powder-bed is the only technology among other inkjet 3DP techniques that has been used for the fabrication of 3D parts using nanocomposites. Other inkjet 3DP methods in which the ink is replaced by melted thermoplastic polymers or a liquid photopolymers have also the potential for the fabrication of 3D nanocomposite structures [21].

The technique is usually used for rapid prototyping because it does not offer printed part with good surface finish and high mechanical strength. The fabricated part usually requires a post-treatment such as presintering or impregnating by a high strength material such as epoxy. The impregnation of a porous printed part by carbon nanofiber (CNF)/epoxy nanocomposites has been studied by Czyzewski *et al*.[57] The porous part was fabricated using a plaster-based powder using a powder bed 3D printer (Z Corporation). **Fig. 3b** shows an optical image of the printed

nanocomposite sample in the volume electrical resistivity measurement. By the addition of only 3 – 4 wt.% CNF, the impregnated part revealed a surface resistivity and volume resistivity of 800 Ω.cm and 200 Ω.cm, respectively. The infiltrating nanocomposite was prepared by stirring and ultrasonication methods. The dimensions of the printed part were 2 mm thickness, 20 mm width and 50 mm length. Azhari et al.[58] investigated the use of the powder bed technology for the manufacturing of 3D porous structures using graphene nanocomposites. The nanocomposite used as the printing powder was a blend of hydroxyapatite (HAP) and graphene oxide (GO) nanoparticles at different loadings of 0.2 wt.% and 0.4 wt.%. The HAP and GO were both hydrophilic and therefore easy to be dispersed and be mixed in water, which reduces the possibility of the nanoparticles agglomeration. The nanocomposite solution was then dried over a hotplate at 90 ºC, resulting in the nanocomposite powder for printing. The proper selection of the nanofillers and the matrix, their proportions and the use of a solution mixing process by stirring enabled to make a printable powder exhibiting good flow-ability. The powder was then placed into the feeding bed of the equipment (Zprinter 310 plus, Z Corporation) and used for the fabrication of 3D cylindrical structures (shown in **Fig. 3c**) with the help of an aqueous binder (Zb^{TM}58, Z Corporation). Layer thicknesses of 100 µm, 125 µm and 175 µm were used to evaluate its effect on the mechanical properties and accuracy of the fabricated parts. The binder saturation level was 100/400 and 100/200 (i.e., ratio of shell binder/core binder). Note that the binder saturation level is defined for the binder concentration in the printing area. The two binder levels (i.e., shell binder and core binder) are important parameters that must be determined before printing. For example, the over saturation may lead to the leakage of the excess binder into the powder bed and affect the fabrication accuracy. The printed structures revealed the best compressive mechanical strength for the case of 0.4 wt.% GO, layer thickness of 125 µm and the binder saturation level of 100/400. Interestingly, the mechanical strength increased significantly from 0.14 MPa for the samples with 0

wt.% GO to ~ 9 MPa (70 times) for the case of 0.4 wt.% GO. The printed structures also showed a considerably improved cold crushing strength (~ 60-fold increase). According to the authors, this type of 3D printed porous nanocomposite structures has potential in load bearing bioapplications and other fields such as optics, supercapacitors, and water purification. They also mentioned that the porosity is necessary for bone implantation in biomedical applications.

3.1.2. Microstereolithography (MSL) techniques

Microstereolithography (MSL), as shown schematically in **Fig. 4**, is a popular conventional maskless method that has been used for several decades for the fabrication of microstructures with a pattern resolution of several microns using photopolymers. The MSL technique enables the fabrication of a 3D microstructure in a layer-by-layer fashion. The first layer is formed when a focused ultraviolet (UV) laser beam scans an uncured photocurable resin on either top (**Fig. 4a**) or bottom (**Fig. 4b**) of a movable stage and selectively cures the resin in the desired locations or paths. When the first layer is formed, the movable stage moves vertically deeper into or out of the resin container and the photopolymerization process is repeated in order to create other layers on top of each other, resulting in a 3D part. The materials constraints such as the need of low viscosity and transparent materials are the main drawbacks of the MSL techniques. The equipment cost may be as low as a few thousand dollars.

Further advances in the MSL led to the development of more precise techniques such as two-photon polymerization with an improved resolution. The two-photon polymerization technique consists in focusing a laser beam into a very small volume of a photopolymer by a high numerical aperture (NA) objective.[59] The technique enables the fabrication of very precise shapes with a resolution down to ~100 nm.[59] Higher resolution (e.g., a few tens of nanometers) is foreseen by the development of novel photopolymers and attractive laser sources.[60] The recent progresses in

the use of the two-photon polymerization 3DP technique for the fabrication of microstructures with high resolution and improved fabrication accuracy have been comprehensively reviewed by Hohmann et al.[61] Zhou et al.[62] discussed processing mechanism and typical setup for the two-photon polymerization technique and also reviewed the parameters influencing the fabrication accuracy in this technique. The fabrication accuracy and the resolution depend on several processing parameters such as the exposure time, the NA of the objective, the laser power and laser wavelength. NA of 1.4 and laser wavelengths in range of NIR are usually used, although, laser wavelengths below the conventional NIR range have been also used (405-540 nm).One of the main limitations of the two-photon polymerization technique is that materials of high optical transparency must be used. For instance, the addition of carbon nanotubes may significantly affect the optical transparency of the resulting nanocomposites which makes it difficult to be used in this technique. Guo et al.[63] reported on the use of a laser direct write technique, based on two-photon polymerization for the fabrication of periodic 3D scaffold using TiO_2-filled polymer nanocomposites. The polymer used as matrix was a UV-curable resin (Ormocer-Ormocore® b59 with 1.8% Photonitiator Irgacure from Microresist Technology GmbH) with refractive index of 1.554 at wavelength of 589.3 nm. The sufficiently high optical transparency of the nanocomposites allowed the fabrication of microscaffold using the two-photon polymerization technique. **Fig. 5** represents the schematic of the fabrication method and an SEM image of a fabricated microscaffold. The scaffold was fabricated by the laser illumination of a film of the UV-curable nanocomposite. The two-photon polymerization setup was composed of a mode-locked frequency-doubled ytterbium-doped glass laser system and a 100× oil immersion microscope objective lens (Zeiss, Plan Apochromat) to focus the laser beam into the nanocomposite materials. Nanocomposites with different TiO_2 nanoparticles loadings (1 – 16 wt.% *sol.*) representing different refractive index were used to fabricate the scaffolds. A laser intensity of 1.4 mW and a

writing speed of 2 mm/s were found to be the optimized printing conditions for the fabrication of mechanically stable structures without any shrinking or collapsing. Here, the addition of TiO_2 nanoparticles not only resulted in mechanical stability, but also keeps the high optical transparency of the nanocomposite at the wavelength required for the two-photon polymerization.[63]

3.1.3. Dynamic optical projection stereolithography (DOPsL)

Dynamic optical projection stereolithography (DOPsL)[64] is another advanced 3DP technology with the same working principles as the MSL. Despite other MSL techniques that work based on maskless approaches (e.g., two-photon polymerization) or use of physical photomasks, the DOPsL utilizes a digital mirror array device (DMD) to produce dynamic virtual photomasks. The layer-by-layer photopolymerization of materials is then carried out by using the dynamic photomasks (one mask for each layer), resulting in complex 3D structures. **Fig. 6** schematically shows the process. A usual setup consists of a light source, a digital mirror array device, a projection lens, and a computer controlled fabrication stage.[64] Different patterns are designed using drawing software (e.g., CAD) and then transferred to the precisely controlled digital mirror to generate virtual micromasks. The resulting images are projected to a photocurable resin. Upon solidification of the light projected area, the patterned layer is fabricated at a time (i.e., under only a single exposure). This unique characteristic provides a significantly higher fabrication speed when compared to the scanning techniques such as the two-photon polymerization technique (e.g., seconds compared to several hours). Complex microstructures having 100 layers with a feature size of 200 μm can be fabricated in ~10 seconds. The fast fabrication speed makes the DOPsL technique suitable for manufacturing of microstructures where high production rates or a large area is of importance. Meanwhile, the resolution of the technique is high (down to 2 μm) and cost of the equipment can be as low as ~$3000.[65] The technique is limited to photocurable materials.

The DOPsL technique has been used for manufacturing of 3D microstructures using nanocomposites for different applications. Gou *et al.*[66] reported the use of this technique for manufacturing of a bioinspired 3D detoxification device using hydrogel nanocomposites for biomedical application, as shown in **Fig. 7**. In this work, polydiacetylene (PDA) nanoparticles with the ability to capture and sense pore-forming toxins were placed in a precise 3D matrix with a desired optimal configuration. The printed 3D matrix was made of a photopolymer poly(ethylene glycol) diacrylate hydrogel which is often used in biomedical applications. **Fig. 7a and 7b** schematically shows the printed pattern of one layer and the detoxification mechanism. **Fig. 7c** and **7d** show a laser confocal microscopy image and an SEM image of the fabricated 3D device, respectively. The PDA nanoparticles were first mixed with a derivative of diacetylene by sonication in order to chemically attach to the 3D matrix. The DMD device was DLP-07 XGA from DLP Technology of Texas Instruments. The results of the dynamic test on the neutralization efficiency for liver-mimetic 3D structure in comparison to the slab control showed that the biomimetic device with a modified liver lobule 3D microstructures is capable of efficient trapping of toxins.[66]

Leigh *et al.*[20] studied the use of the DOPsL technique for the fabrication of a flow sensor device. **Fig. 7e** and **7f** presents the schematic of the sensor operation and a photo of the fabricated device. The device was composed of a 3D printed acrylic-based photopolymer (R11, Envisiontec) body and a nanocomposite impeller. The nanocomposite material used to fabricate the impeller was a blend of a two-part polymer (1,6 hexanediol-ethoxylate diacrylate and dipentaerythritol penta-/hexa-acrylate, 1:2 weight ratio), a photoinitiator (5 wt.%, Irgacure 784, Stort Chemicals) and magnetite Fe_3O_4 nanoparticles (50 nm-diameter, Sigma Aldrich) with nanoparticles loading of 25 wt.%. The printing setup used was a home-made MSL system composed of an LED light, a DMD projector (Compaq MP1800), focusing optics, a mirror and a 3-axis positioning stage (Aerotech UK (*x* and *y*) ALS130-100 (*z*) ALS130-050). The fabricated device was successfully tested by

connecting it to a compressed air line and monitoring the sensor output (by rotations of the impeller) using the AMR sensor, as shown in **Fig. 7e**. In this work, the flow rate was remotely measured using the magnetic AMR sensor. This type of sensor devices might have potential in microfluidics and micropneumatics.[20]

3.2. 3DP with extrusion-based direct-write approach

Extrusion-based direct-write techniques are known as cost-effective techniques that offer huge opportunities for 3DP of a wide variety of materials including multifunctional nanocomposites. These techniques which are based on computer-controlled deposition of continuous ink filaments allow the rapid fabrication of 3D microstructures through a layer-by-layer building sequence without the need for expensive accessories, tooling and masks.[67, 68] **Fig. 8** schematically illustrates the simple concept of these 3DP techniques through which a 3D structure is built by means of a computer-controlled robot that moves a dispensing apparatus along the x, y and z axes. The first layer of a 3D structure is fabricated by the deposition of the ink material on a substrate. The position of the deposition nozzle is then incremented in z-direction for the fabrication of following layers in a continuous manner. Accurate fabrication of a pre-designed structure and its resolution depend on the rheological behavior of the material and the resolution of the printing equipment.[67, 69] For instance, high viscosity of materials and nanofiller clusters may cause processing problems such as nozzle clogging[70, 71]. In this section, recent advances in 3DP of nanocomposite materials using the extrusion-based direct-write techniques are reviewed with an emphasis on the printing capability and material requirements. For all the extrusion-based 3DP methods, an increase of material rigidity right after extrusion is a key factor for filament shape retention.[67] Therefore, the mechanisms associated with each method are also discussed.

3.2.1. Direct-write (DW) assembly – 3DP of rheologically-tailored inks

Direct-write (DW) assembly is an ink-based technique that relies on the deposition of the rheologically-tailored ink filament made of colloid, nanoparticle or organic materials to build structures in layer-by-layer manner. Several works have been reported by Lewis and co-workers on the fabrication of complex 3D self-supported (i.e., spanning) microstructures by controlling the materials rheological behavior. A shear thinning behavior (i.e., a decrease of viscosity with an increase of shear forces inside the nozzle) is found to be a favorable case for the layer-by-layer fabrication of microstructures with spanning feature like periodic scaffolds.[67, 68, 72] The shear thinning behavior enables the materials to be extruded through fine nozzles and, on the other hand, possess enough shear elastic modulus and shear yield strength to retain its shape. However, a further increase of rigidity is needed to fabricate very long spanning structures or freeform structures such as helices and spirals. The resolution of these techniques can be very high (~2μm). The cost of the direct-assembly techniques significantly depends on the cost of equipment and its working resolution. It may vary from $1000 for a simple home-made setup to >$15000 for commercial dispensing robots.

Campton *et al*.[15] reported 3DP of cellular composites representing significant mechanical performance through the rheology modification of a filled epoxy resin by the incorporation of nanoclay platelets. **Fig. 9a and 9b** schematically shows the printing process and manufactured composite part. The Newtonian epoxy resin changed to a viscoelastic fluid by the addition of about 5 wt.% nanoclay. The epoxy nanocomposite ink was also filled with milled carbon fiber (diameter and mean length of 0.65 μm and 12 μm, respectively) and silicon carbide whiskers (diameter and mean length of 10 μm and 220 μm, respectively) for further improvement of mechanical properties of the final printed part. Direct-write technique was then employed to manufacture hierarchical wood-inspired composite structures with controlled composition, geometric shape and complexity.

Several architectures with different geometries were fabricated with a wall thickness of about 200 μm and height of >2 mm (equal to 20 layers) using nozzle diameters ranging from 200 μm to 610 μm. The 3DP equipment was composed of an Aerotech 3-axis positioning stage (Aerotech, Inc.) and an Ultimus V pressure box (Nordson EFD) as a pressure regulator. The 3DP of these nanocomposite materials also enabled aligning high aspect ratio fibers along the printing direction that significantly affected the composite mechanical performance. **Fig. 9c** shows the optical image of the printed structures representing the alignment of the fillers. Shear and extensional flow fields inside the nozzle were believed to be responsible for the preferred fillers orientation. This printing-induced orientation capability can be used for manufacturing engineered structures with optimal mechanical properties. For instance, the printed composites exhibited Young's modulus values as high as ~24.5 GPa which is close to wood cell walls, twice the value of the best commercial printed polymer composites and an order of magnitude higher than those of printed thermoplastic composites.[15]

Ahn *et al*.[73] reported planar and 3DP of electrically conductive nanocomposite inks containing silver nanoparticles with printing resolution of ~ 2 – 30 μm. The highly concentrated metallic ink containing ~85 wt.% of silver nanoparticles with a diameter ranging from 20 – 50 nm were first synthesized. Ethylene glycol was added to the ink in order to control the ink viscosity and make it suitable for the 3DP. It was found that the ink viscosity increases with increasing the silver ink concentration in the resulting nanocomposite mixture. The relatively low amount of silver ink (e.g., <70 wt.%) in the mixture resulted in an unsuccessful printing due to material spreading. An ink with the silver concentration of 70 – 85 wt.% was found to be necessary for the fabrication of planar and 3D printed structures. After adjusting the ink rheology, several spanning and self-supported features were fabricated by the DW-3DP of the nanocomposite inks through fine nozzles with the internal diameter as small as 0.5 μm. **Fig. 10** represents several optical and SEM images of

the printed planar and spanning conductive structures for electronic and optoelectronic applications. **Fig. 10a** shows SEM images of 2D lines of conductive microelectrodes with a line width of ~ 2 μm and a thickness of 1.4 μm, deposited using a nozzle with an internal diameter of 1 μm. **Fig. 10b** shows optical and SEM images of silver grids printed as a function of line pitch using a 5 μm nozzle on a flexible polymer film. According to the authors, this type of transparent conductive films exhibits high potential to be an alternative for conductive oxide materials. SEM image of a complex 3D periodic conductive scaffold fabricated using a 5 μm nozzle is depicted in **Fig. 10c**. **Fig. 10d** shows SEM image of the spanning metallic microelectrode deposited onto a silicon solar microcell array for 3D photovoltaics applications. 3D spanning electrodes was also used for the fabrication of light-emitting diodes (LEDs). **Fig. 10e and 10f** shows SEM images of spanning or freeform conductive interconnects for an LED array, representing the possibility of printing of multilayer interconnections. Thermal annealing at high temperatures (250°C - 550°C) significantly enhanced the electrical conductivity of the printed structures as a result of material densification (up to 30 % of shrinkage). For instance, the resistivity measurement revealed a value of ~10^{-5} Ω.cm for the microelectrodes upon annealing at 250°C for less than 30 min.[73]

A few studies have reported on the use of DW assembly technique combined with an infiltration approach for manufacturing of engineered microstructured nanocomposite macrostructures.[31-33, 74] **Fig. 11** illustrates different steps of the fabrication process and representative optical images of the manufactured structures. These nanocomposite structures were manufactured by the infiltration of uncured nanocomposite materials into an empty 3D interconnected microfluidic network.[31, 74] The microfluidic network was first fabricated by layer-by-layer direct deposition of a sacrificial ink onto an epoxy substrate, resulting in an ink-based scaffold 3D structure, as schematically shown in **Fig. 11a**. The sacrificial ink was a 40 wt.% binary mixture of a microcrystalline wax (SP18, Strahl & Pitstch) and a petroleum jelly (Lever Pond's). The printing setup consisted of a computer-

controlled robot (I & J2200-4, I & J Fisnar) and a dispensing apparatus (HP-7X, EFD). Each layer was alternatively oriented along and perpendicular to the scaffold longitudinal, *x*, axis. The number of filaments deposited along the longitudinal direction gradually decreased from the outer layers to the center of structure in middle layers. The structure was then encapsulated using a liquid uncured epoxy resin (**Fig. 11b**). Upon the solidification of the encapsulating resin, the empty microfluidic network was finally achieved by the removal of the sacrificial ink by melting (**Fig. 11c**). **Fig. 11d** schematically illustrates the dimensions of the unfilled microfluidic structure, followed by its infiltration using uncured carbon nanotube-based nanocomposites. Epoxy (e.g., EPON 862, EPON 828, Hexion Inc.) and urethane-based (e.g., NEA 123MB, Norland Products Inc.) resins were mixed with the nanotubes at different loadings (0.5 – 1 wt.%) to prepare the infiltrating nanocomposites. A mixing strategy including nanotubes' surface treatment, ultrasonication and high shear mixing in a three-roll mill mixer was used to efficiently disperse nanotube into the resins before the infiltration. **Fig. 11e** shows an isometric view of the manufactured nanocomposite structure after curing of the infiltrated nanocomposites (EPON 862 and a nanotube load of 0.5 wt.%). **Fig. 11f** is an optical image the manufactured part cross-section, showing the configuration of the infiltrated nanocomposites. This approach enabled orienting the nanotubes along the infiltration axis and also positioning the nanocomposite into a designed pattern.[31, 74] For example, here the pattern was designed in order for the nanotubes to be positioned at higher stress regions to offer better performance under flexural solicitation. According to the authors, this novel manufacturing method allows the utilization of different nanocomposite materials in order to design multifunctional nanocomposites for potential applications such as internal damage detection of the composites and embedded organic flexible electronics.[74]

Aissa *et al*.[75] reported the use of the infiltration approach for manufacturing of microvascular-based second generation of self-healing nanocomposite materials with aiming at improving their

mechanical performance. As shown in **Fig. 12a**, a liquid nanocomposite consisting of SWCNTs and 5-ethylidene-2-norbornene (5E2N) as healing agent was infiltrated into the 3D microfluidic network. During the fabrication of the microfluidic network, ruthenium Grubbs catalyst was added to the epoxy and used for the encapsulation of the sacrificial ink structure. The concept of these self-healing materials is that, upon creation of any damage to the 3D-filled structure in forms of crack and holes, the nanocomposite healing agent flows to the damage zone and reacts with the locally available catalyst. Upon a quick reaction, the damaged structure is healed so that its mechanical performance is comparable with the undamaged structure. The 5E2N liquid monomer (Sigma Aldrich) was found to be a proper healing agent with an excellent monomer conversion (i.e., polymerization in presence of the catalysts) rate at a short period of time (less than 5 min). **Fig. 12b and 12c** shows the optical top-view images of a microfluidic-based structure filled with nanocomposite right after the impact event and after 30 min, respectively. A heating at 60 ºC was also performed to accelerate the healing process, resulting in complete solidification and healing of the damaged zone. The authors reported that the addition of only 2 wt.% nanotubes to the healing agent significantly improved the Young's modulus (from 3.6 GPa to 14 GPa) and hardness (from 0.4 GPa to 3.6 GPa) of the local healed zone, measured in microindentation test. The incorporation of nanofillers helps further improvement of the overall mechanical performance of the filled structures for applications such as self-healing composites used in aerospace and space industries.[75] Since the microvascular networks are fabricated by 3DP, the flexibility of 3DP techniques enables to fabricate high-efficient new products with an optimized geometry. For instance, the main issue of long healing time related to this type of self-healing materials consisting of two interpenetrating microvascular network has been addressed by 3DP of a third interdigitated microvascular network.[76]

3.2.2. Fused deposition modeling (FDM) or heat-assisted 3DP (HA-3DP)

Fused deposition modeling (FDM) is one the most popular 3DP methods because it is widely used in commercial 3D printers both in the industry and academia. **Fig. 13** schematically represents the FDM method[77] through which various geometries can be fabricated using different materials such as polymers, metals and ceramic or metal-filled polymers.[78] The FDM is a cost effective method capable of making objects with a resolution of ~40 μm. This method is a heat-assisted manufacturing process in which the printing material, usually thermoplastic polymers in the form of spooled filament, is heated up inside a printing head to a desired temperature (e.g., close to its melting point) and then is extruded from a nozzle. The extruded material is deposited onto a substrate to build a 3D structure in a layer-by-layer manner using a positioning stage. Short after the deposition, the printed material cools down and solidifies. This technique is capable of fabricating 3D structures with spanning or freeform features.[71] The most frequently used polymers are thermoplastics such as PLA and acrylonitrile butadiene styrene (ABS).[79] Despite several advantages offered by the FDM such as cost effectiveness and the diversity of the materials that can be used, this method exhibits some drawbacks such as material degradation at high temperature and high viscosity of molten materials. Material requirement (e.g., thermal and rheological properties) is another drawback of the FDM method. Interestingly, it has been observed that the incorporation of high aspect ratio nanofillers to the printing materials can help modify their rheological behavior and make it easier to extrude them through a finer deposition nozzle [44]. The cost of the FDM printers varies from $200 - $330000.[71]

Castro *et al.*[80] reported the design and fabrication of a bioactive nanocomposite scaffold with improved osteochondral regeneration properties for tissue engineering application in a printing-encapsulating-dissolving approach. A scaffold with a desired porosity (40 % in-fill density) was first fabricated by the FDM printing of a polystyrene polymer using a table-top FDM 3D printer

(Solidoodle©). **Fig. 14a and 14b** shows side view and top view optical images of the fabricated polymeric scaffold. An extrusion nozzle with an internal diameter of 325 μm and a multiplier of 0.6 were used to fabricate the 3D scaffold with the filament diameter of ~240 – 270 μm. The fabricated scaffold was then encapsulated using uncured nanocomposite materials. The nanocomposite materials contained nanocrystalline hydroxyapatite (nHA) with a grain size possessing a length of 50 – 100 nm and a width of 20 – 30 nm. Upon photocuring of the encapsulating nanocomposite materials under an UV exposure time of 8 minutes, the polystyrene scaffold was dissolved and removed using a 33 vol.% solution of D-limonene, resulting in a 3D interconnected microfluidic network. **Fig. 14c** shows an SEM image of a representative highly porous interconnected scaffold. The diameter of the resulting channels was equal to the dissolved polystyrene filaments. The flexibility of the FDM method enables to fabricate the 3D porous nanocomposite microstructure with the desired porosity, simply by altering the nozzle diameter and the extrusion multiplier. The presence of nHA nanoparticles inside the biomimetic 3D structure not only efficiently improved bioactivity (i.e., increased the cell adhesion), but also led to a considerable enhancement of compressive strength of the fabricated scaffold. For instance, compared to the structure fabricated using the pure polymer, the addition of 60 wt.% nHA nanoparticles led to 61% and 87% increase in compressive modulus and compressive strength of the nanocomposite-based structure, respectively.

Bouchaar *et al.*[81] developed a heat-assisted 3DP (HA-3DP) method with the same principle as the FDM. Instead of positioning stages that are used in FDM, a computer-controlled robot was used in the HA-3DP. Another difference is that the nanocomposite pellets were fed into the dispensing head of the HA-3DP and pushed through the nozzle by a pressurized piston. The authors then studied the capability of the HA-3DP method by using nanoclay/PLA nanocomposites for the manufacturing of 3D scaffold with potential application in tissue engineering. **Fig. 15** represents different aspects of their work. The HA-3DP used here was composed of a commercially available

computer-controlled robot (I & J2200-4, I & J Fisnar, and JR Point dispensing software) consisting of a stage moving along the *x*-axis and a robot head moving in the *y-z* plane. The dispensing apparatus that carried the nanocomposite material was mounted on the robot head. As shown in **Fig. 15a and 15b**, the apparatus consisted of a metallic syringe surrounded by heating elements, a metallic nozzle, a metallic piston to apply the extrusion pressure with the help of a pressure regulator (HP-7X, EFD) and a pneumatic fluid dispenser (UltraTM, EFD). The total cost of the robot and the accessories is ~$15000. The nanocomposite material was in the form of pre-mixed pellets, prepared by mixing nanoclay and the PLA polymer by melt mixing in a twin screw extruder. **Fig. 15c** shows an optical image of the extrusion nozzle during the deposition of a filament. **Fig. 15d and 15e** shows the optical and SEM images of a 6-layer scaffold fabricated by this technique using the PLA nanocomposites (2 wt.% of nanoclay), respectively. The filament's diameter, its length in each layer and the height of the scaffold were ~330 µm, ~20 mm and ~800 µm, respectively. The deposition speed and pressure were 6 mm/s and 1.4 MPa, respectively.

Ahmadi *et al*.[82] studied the acoustic performance of 3D printed nanocomposite earmuff macrodevices. In their work, acrylonitrile butadiene styrene (ABS)/nanoclay nanocomposites (4 wt.% of nanoclay) were prepared in a twin screw extruder and used as nanocomposite filament for the fabrication of single and double cup earmuffs using a FDM 3D printer (Creater, Leapfrog). **Fig. 16a** shows a photo of a representative fabricated earmuff and **Fig. 16b** shows the acoustic test fixture in objective noise attenuation test. The 3D printed nanocomposite earmuff showed higher performance in terms of insertion loss and noise reduction rating when compared to the one fabricated using the pure ABS.

Leigh *et al*.[83] reported on the development of a low-cost conductive nanocomposite material as feedstock for a FDM-based 3D printer (BFB3000, Bits from Bytes Ltd) for the fabrication of innovative electronic sensors capable of sensing mechanical flexing and capacitance changes. The

printing material was a blend of a biodegradable low-melting point (60ºC) thermoplastic polymer, polycaprolactone (PCL), and carbon black with 15 wt.% loading. The feedstock material was a 3 mm wide filament, prepared by solution mixing (DCM solvent) followed by solvent evaporation, warming and rolling of the dried material between two glass plates. **Fig. 17** represents the fabricated functional devices that work based on the piezoresistive behavior of nanocomposite materials, here the carbon black/PCL nanocomposite. **Fig. 17a and 17b** shows photos of a fabricated flex sensor composed of a single 2D filament with two printed sockets at both ends of the filament in inflexed and flexed status. The change of the sensor resistance under flexion was measured, as shown in **Fig. 17c**. A repeatable (over 50 times) trend with the resistivity change of ~4% was observed. The authors believed that this type of materials might find applications in structural health monitoring. **Fig. 17d** shows photos of a capacitive device composed of 3D printed capacitive buttons. When the printed conductive pad is touched, the increase of capacitance of the pad is sensed and can be used as an actuator. Another example of 3D printed devices is a printed smart mug containing two printed nanocomposite lines on the side (**Fig. 17e**.). The device is capable of sensing the volume (or level) of a liquid (e.g., water) that fills the mug. The printed nanocomposite filaments were connected to a capacitive meter by which the capacitance variation was measured. A linear relationship was observed for the change of capacitance with added volume of water.

3.2.3. *Liquid deposition modeling (LDM) or solvent-cast 3DP (SC-3DP)*

The LDM[84] and SC-3DP[9, 12] are two recently developed printing methods which use the same printing principle. These two methods consist in the direct deposition of polymer or nanocomposite solutions which is extruded through a deposition nozzle. Schematics of these two fabrication processes are shown in **Fig. 18**. **Fig. 18a** shows the deposition of a 3D printed filament in a

freeform manner and the LDM setup and also a representative photo of a fabricated 3D freeform microstructure with a filament diameter of 100 μm and a spanning length of a few mm. **Fig. 18b** shows a photo of dispensing syringe and the fixture. The equipment is originally a table-top commercial 3D printer (Futura Elettronica) in which the printing head was replaced by a solution dispensing system. A computer-controlled stepper motor (NEMA17) was used to regulate the pressure on the syringe piston. **Fig. 18c** schematically represents the SC-3DP method and the material solidification mechanism. In both methods, the polymer or nanocomposite materials are first dissolved in an appropriate solvent, usually a volatile solvent like dichloromethane (DCM). This significantly decreases the viscosity of the material and facilitates its extrusion through a very fine nozzle with an internal diameter as low as 10 μm. The extruded material solidifies in seconds upon the fast evaporation of solvent and retains its filamentary shape (**Fig. 18c**). Both techniques require almost similar equipment which are mainly composed of a syringe filled with the material solution, a micronozzle, a pressure regulator and a computer-controlled moving stage.[9, 84]

These two solvent-assisted 3DP methods have been used for the fabrication of nanocomposite microstructures for potential applications in microelectronics and sensors. **Fig. 19a** and **19b** shows top-view and side-view SEM images of a nanocomposite scaffold fabricated by the LDM method, respectively. The nanocomposite was a blend of PLA and multi-walled carbon nanotubes (MWCNTs) with loading of 1 wt.%. Magnetic stirring followed by ultrasonication were used to mix MWCNTs and PLA in DCM. The conductivity of this nanocomposite scaffold allows lighting up an LED light by using a 3V CR2032-type watch battery, as shown in **Fig. 19c**. This type of conductive scaffold might find applications in microelectronics.[84] **Fig. 19d** shows SEM image of a freeform nanocomposite microspiral fabricated using the SC-3DP method. Guo *et al.*[12] reported the SC-3DP fabrication of freeform spirals using MWCNTs/PLA nanocomposites and tested them in an electrical circuit to light up an LED light (**Fig. 19e**). They also tested this type of helical

microstructures for liquid sensing applications. The nanocomposite liquid sensor was fabricated using a 30 wt.% PLA in a DCM solution and a nanotube loading of 5 wt.%. The conductivity of the spiral was measured in a two-probe setup and showed a value of about 23 $S.m^{-1}$. When the sensor is dipped into a solvent, the solvent is trapped inside the spiral (**Fig. 19f**) and the electrical conductivity changes as a result of disconnection of the conductive CNT network caused by polymer swelling in the solvent. Owing to its unique geometry, the liquid sensor featured an excellent sensitivity and selectivity for several solvents such as acetone, toluene and ethanol, even for a short immersion time (seconds).[12]

The printability window of 3D microstructures in these two solvent-assisted methods varies from a geometry to another (e.g., freeform or supported) and depends on several processing parameters and the materials type. As reported by Guo *et al.,*[9, 41] the processing window is narrower for the manufacturing of 3D freeform structures. The resolution of fabricated structures and filament diameter depend on the resolution of the dispensing robot, the rheology of the materials and the diameter of the nozzle. The minimum achievable diameter of the extruded filament has been reported as ~100 μm for manufacturing of freeform spirals in the SC-3DP method.[9] In any case, in order for the extruded filament to retain its shape after printing, the proportion of solvent, polymer and nanofillers should be properly set to allow the easy material extrusion and quick drying. The nanofillers concentration is a very important factor since their addition at high loadings might cause processing problems such as increase of viscosity and nozzle clogging as a result of nanofillers agglomeration. Although the LDM and SC-3DP methods offer several benefits such as simplicity, room temperature processing and low viscosity of the materials, they have a few limitations and drawbacks. For instance, the materials used for this type of printing are limited to the polymers with the ability to dissolve in low boiling points solvents. This is necessary for a fast solvent evaporation in order for the material to solidify and retain its printed

shape. To the best of our knowledge, only the nanocomposite solution containing DCM, PLA and MWCNTs has been used to fabricate microstructures in these methods. However, other polymers and nanocomposites can be adapted to these two methods. The total cost of the dispensing robot and the accessories for SC-3DP is ~$15000 while the cost of the LDM setup depends on the cost of printer used (≥$1000).

3.2.4. Conformal 3DP (C-3DP)

The C-3DP method is another extrusion-based printing method which consists of the deposition of ink filaments onto conformal surfaces (e.g., curvy shapes).[71, 85] The C-3DP consists of a computer-controlled dispensing system that extrudes the ink directly onto a conformal surface. The printed material is entirely supported by the substrate, enabling a very precise fabrication of complex patterns. 3D supported structures are fabricated by a relative movement of the dispensing nozzle and the substrate. The fabrication resolution varies from a method to another and strongly depends on the resolution of the dispensing robot and/or the stage that moves the substrate. **Fig. 20a** and **20b** represents schematic and optical image of conformal printing of a helical microstructure through the deposition of an ink filament (PLA solution) onto a rotating mandrel. In this particular setup, a MICOS stepper motor was used to rotate the mandrel and move it along the x axis with a resolution of 0.4 μm.[85] The shape and the size of microstructures can be controlled by the nozzle's diameter, the extrusion pressure, the diameter and rotation speed of the mandrel and the displacement speed of the extrusion nozzle. The main drawback of the C-3DP is that the shape of the structure may be limited to those that can be taken off the mandrel after printing.[71] The cost of this technique depends on the cost of dispensing setup (e.g., stage and pressure regulator).

Adams *et al*.[11] reported the conformal printing of conductive nanocomposite inks containing silver nanoparticles on curvilinear surfaces. The ink material was a nanocomposite containing 72

wt.% of silver nanoparticles (a mean diameter of 20 nm), poly-acrylic acid and ethylene glycol[86]. A very high resolution 3-axis positioning stage with a positional accuracy of 50 nm (ABL 9000, Aerotech) was used as the material dispensing equipment. The extrusion nozzle used were either a 100 μm nozzle (7018462, Nordson EFD) or 30 μm (pulled-glass capillary, P-2000, Sutter Instrument) while the printing speed varied between 0.1 – 1 mm/s. Since the deposition on the non-planar surfaces adds fabrication complexity, the nozzle was bent at angles (10º – 45º) to facilitate printing, mostly for the case of smaller diameter nozzles (e.g., 30 μm). The authors demonstrated C-3DP of conductive antennas on a hemispherical glass substrate in the form of conductive meander lines as shown in **Fig. 20c**. The fabricated antennas exhibited a high working efficiency of 68% – 72% which was comparable to the theoretically predicted value (66%). According to the authors, the antennas fabricated using the C-3DP exhibited a huge potential for wireless communications.

Vatani *et al.*[87] studied the use of the C-3DP for manufacturing of multilayer tactile piezoelectric sensors using nanocomposites. The nanocomposite material was a blend of a photocurable resin (TangoPlus FullCure®930, Objet Geometries Inc.) and MWCNTs (NanoLab) with a loading of 0.5 wt.%. The dispensing equipment was a computer-controlled precision XYZ stage (Aerotech) that moved a microdispensing head (PCD3, GPD Global. Grand Junction Co.). **Fig. 20d** shows an optical image of the manufactured tactile sensor. The sensor was composed of two perpendicular sets of eight sensing elements printed onto conformal substrates and each set separated by an insulating polymer layer. The fabrication process began with the deposition of the nanocomposite filaments as sensing elements on top of a curvy substrate. The intermediate insulating layer was casted on top of the deposited filament and the second set of the filament was printed onto the intermediate layer, followed by casting of the top insulating layer to entirely embed the nanocomposite sensing elements. The diameter of nanocomposite filaments was 1 mm with a

filament spacing of 3 mm. The deposition speed, the nozzle internal diameter and the distance between the nozzle and the substrate were 10 mm/s, 535 μm and 350 μm, respectively. The curvy substrate was made of a highly stretchable polyurethane rubber (SkinFlexIII, BJB Enterprises) as the main body of the sensor. The nanocomposite material which was used as sensing elements of the sensors was also stretchable exhibiting an elongation of 170% - 220%. With the same principle as other nanocomposite electromechanical sensors, the fabricated tactile sensor was based on the electrical conductivity variations caused by nanofiller rearrangement upon an applied external force. The unique multilayer feature of the fabricated tactile sensor enabled detection of external forces locations on the sensor surface in a contact force experiment. The multilayer configuration of the sensor increased the number of sensing taxels with the ability to detect a 2D location of an applied force.[87]

3.2.5. UV-assisted 3DP (UV-3DP)

The UV-3DP, developed by Lebel *et al.*,[6] is another emerging extrusion-based direct-write technique exhibiting a huge potential for manufacturing of nanocomposite microstructures with freeform and supported features. The UV-3DP technique consists in the robotically-controlled deposition of an ink filament while the extrusion point is moved in three directions. The uncured viscos liquid material is photopolymerized within seconds after extrusion under UV exposure. The mechanism for solidification of filament (i.e., sufficient increase of filament's rigidity) is resin crosslinking which is caused by photopolymerization. Therefore, the ink material, either pure resins or nanocomposites must be UV-curable. **Fig. 21a** represents a schematic of the UV-3DP fabrication of a freeform filament. The UV light-emission setup is mounted on the robot head and follows the extrusion point. Different configurations of the UV setup were designed to deliver the light in a focused zone starting right after the filament is extruded (**Fig. 21a**). In the latest design, as shown in

Fig. 21b, a set of six optical fibers arranged in a circular pattern were used for the delivery of the UV light close to the tip of the extrusion micronozzle (Precision Stainless Steel Tips, EFD). The light was generated by two high-intensity UV light-emitting diodes (LED, NCSU033A, Nichia) having a wavelength centered at 365 nm. The fabrication setup may cost about $15k – $20k. For accurate fabrication of 2D patterns, 3D self-supported and 3D freeform microstructures, materials criteria have to be met and also the manufacturing parameters have to be properly chosen. Farahani *et al.*[70] reported a systematic study on the effects of manufacturing conditions of the UV-3DP technique and drew a processing map for successful fabrication of structures with different geometries. Similar to other extrusion-based 3DP techniques, the materials with moderate to high viscosities featuring shear thinning behavior are necessary to obtain stable filament after material extrusion. Pure UV-curable resins usually exhibit low viscosity and Newtonian rheological behavior and are not suitable for the UV-3DP technique. Unfilled commercially available resins such as acrylate-based or epoxy-based resins which are the most-commonly used UV-curable materials exhibit a fast reactivity, but their viscosities are as low as 2 Pa.s.[88] Such a low viscosity leads to sagging of the extruded materials prior to solidification under the UV illumination.[70] Several studies reported the sufficient increase of viscosity by the addition of nanofillers such as carbon nanotubes and silica nanoparticles that enabled a successful UV-3DP.[71] Therefore, the addition of nanofillers not only makes the materials suitable for the UV-3DP method, but also adds functionality (e.g., conductivity) to the printed materials, which is very important for various applications in MEMS and microelectronics.

The filament rigidity might be sufficient for self-supported spanning structures, however, a further increase of rigidity over a short period of time is required for the fabrication of freeform structures like helical geometries. This rigidity increase is provided by the photopolymerization of the filament under UV exposure. After finding a proper material choice, the extrusion pressure and

the speed have to be matched to achieve the critical conversion rate, which may vary depending on the desired geometry. Since the fabrication of freeform structures needs high material conversion for self-standing of the structure, the processing window is much narrower when compared to the self-supported structures.[70]

Fig. 22 shows several representative nanocomposite microstructures either with plain 2D, spanning or freeform features, manufactured using UV-3DP method. Fig. 22a is a deposited 2D line network similar to traditional strain gauges.[17] The material used was a UV-curable epoxy (UV-DC80, Master bonds) mixed with 1 wt.% SWCNTs. The high electromechanical sensitivity of nanocomposite-based sensor is advantageous over the traditional strain gauges. High GF of a few dozen can be achieved for the nanocomposite sensors while the traditional metallic strain gauges offers a GF of ~2. Fig. 22b shows an optical image of a nanocomposite coupon which consisted of three microfibers suspended between two nanocomposite tabs. The electromechanical performance of the fabricated coupon was assessed under tension for applications as strain sensors. The sensor exhibited a high GF of ~22. Fig. 22c shows that the suspended microfibers have a circular cross-section with a diameter of 120 μm. The suspended feature of the fibers may help minimize the effect of local cracks which may cause disconnection of the electrical pathways.[17]

Fig. 22d shows a SEM image of a triangular array of three helical nanocomposite microcoils with high potential for applications such as load bearing MEMS components.[6] The material used here was a mixture of a UV-curable urethane-based resin (NEA 123MB, Norland Products Inc.) and 0.5 wt.% SWCNTs. The mechanical performance of the triangular nanocomposite microcoils network was evaluated under compression. A quasi-linear response was observed with a rigidity of ~11.7 mN mm^{-1}. The desired mechanical properties of these microcoils could be easily achieved by using other resins with higher mechanical performance and also by optimizing the geometry characteristics of the microcoils. Fig. 22e shows a SEM image of a displacement sensor composed

of four identical helical microcoils, arranged in a rectangular array for structural stability. The microcoils were fabricated through UV-3DP of the UV-curable epoxy nanocomposites containing 1 wt.% SWCNTs. This type of 3D nanocomposite sensors can be geometrically optimized in order to show very high sensitivity and may find different applications due to its lightness as well as feasibility of the direct printing of sensing elements onto the structure.[17, 71] For the nanocomposite-based sensors with either 2D or 3D geometries, high aspect ratio (i.e., length/diameter) nanofillers such as carbon nanotubes play the role of large-surface sensing elements so that their re-arrangements under an external mechanical disturbance induce electromechanical sensitivity which strongly depends on the spatial distribution and concentration of the nanofillers.[89] The nanocomposite helical microstructures may also have potential to accurately sense biomaterial solutions[90] or measure liquids flow rate[91] only by monitoring the variation of their electrical conductivities when they are subjected to chemical or mechanical disturbances. Compared to the 2D devices, the 3D sensors offer a high surface area and mechanical flexibility.

The UV-3DP method was also used for the fabrication of 3D periodic scaffolds, as shown in **Fig. 22f**.[92] The periodic scaffolds are frequently used in tissue engineering and might have other applications such as in liquid sensing due to their large surface area. In these applications, filament spacing (or porosity of the structure) is of great importance and has a direct effect on the capability of the manufactured device. The flexibility of the UV-3DP method allows the fabrication of scaffolds with a desired overall size, filaments length and diameter for targeted applications. It is worth mentioning that the significant increase of filament rigidity in the UV-3DP method prevents sagging of spanned filament that enables fabricating the scaffold featuring long filament spacing. A filament spacing as high as 100 times the filament diameter has been reported for the UV-3DP method while this value is about 10 for the printed fugitive ink filament.[70]

Aissa *et al*.[93] reported on the UV-3DP and transport properties of a field effect transistor (FET) consisting of SWCNTs-filled nanocomposite microfilaments as active channels (**Fig. 23**). The nanocomposite were first prepared by mixing of a urethane-based UV-curable resin (NEA 123MB, Norland Products Inc.) and SWCNTs with different loadings ranging from 0.1 wt.% to 2.5 wt.%. To fabricate the FET 2D device, the nanocomposite filaments with diameters of $100 - 500$ μm were directly deposited onto SiO_2/Si substrates, patterned with Ti/Mo (10/250 nm thick) electrodes. **Fig. 23a** schematically illustrates the deposition of a nanocomposite filament using the same setup shown in **Fig. 21a**. **Fig. 23b** schematically shows the principle of the FET device in which the metallic Ti/Mo, underneath the nanocomposite filaments were used as the source and drain electrodes. The p-doped silicon substrate was used as a back gate electrode. The authors showed that the FET performance of such transistors depends on the nanotubes concentrations as well as the filaments' diameter. **Fig. 23c** is an optical image of a printed nanocomposite filament (0.5 wt.% of SWCNTs and filament's diameter of 200 μm). The UV-3DP method enabled to precisely control the diameter and length of the filaments by the variation of the deposition speed and the extrusion pressure. The results revealed that all the filaments with the nanotubes loading of ≤1.5 wt.% behave as a FET with p-type transport. The FET device fabricated through UV-3DP of nanocomposites with the lowest nanotube loading (0.1 – 0.2wt.%) exhibited high performance with FET characteristics of I_{on}/I_{off} ratio of $\geq 10^5$ and a maximum on-state current of as high as 70 μA. The I_{on}/I_{off} ratio decreased by the increase of nanotubes' loadings. For the cases of nanotubes loadings of ≥2 wt.%, no significant increase of electrical conductivity was observed, indicating that the electron transfer mechanism changed so that it was no longer p-type. The flexibility of the technique to control the channels (i.e., nanocomposite filaments) diameter and easier fabrication compared to nanotube-based devices are the main advantages of 3DP of nanocomposite FET devices.[93]

A systematic study on the effect of nanofiller loadings on rheological behavior, tensile mechanical properties and printability of the UV-3D printed nanocomposite materials has been recently reported by Postiglione et al.[94] Two types of fumed silica nanoparticles with different particle size and size distribution (10-100 nm and 8-20 nm) and also nanoclay platelets (6-8 μm characteristic length) were used as fillers and mixed with a UV-curable resin. The resin was a blend of trimethylolpropane ethoxylate triacrylate (TMPETA, average M_n ~560) and a photoinitiator (2-hydroxy-2-methyl-1-phenyl-propan-1-one, 3 wt.%). Rheological results showed a Newtonian response for the pure resin and a shear-thinning behavior for the nanocomposites. Viscosity-shear rate curves were then fitted with a power-law equation ($\eta = K\dot{\gamma}^{n-1}$ where $\eta, K, \dot{\gamma}$, and n stand for viscosity, consistency index, shear rate and power-law index, respectively). The progressive addition of nanofillers increased K depending on the type of nanofillers and their concentrations (e.g., 10-fold increase between 15-30 wt.% of fumed silica with the size distribution of 10-100 nm). The authors showed that only the nanocomposites with sufficiently high values of K (>550 Pa.s^n) exhibit optimal printability properties (i.e., optimal printing resolution and well-defined printing features). They also showed that the mechanical properties of the UV-3D printed dumbbell specimens depends on the printing direction, suggesting the capability of the 3DP to tailor mechanical properties of 3D printed structures. A home-made UV-3DP setup consisted of a 3Drag 1.2 benchtop printer (Futura Elettronica, Italy), a syringe dispenser and five UV LEDs (emission peak at 365 nm, Aftertech SAS, Italy) was employed to fabricate 3D microstructures. The cost of this home-made setup can be as low as ~$1500. **Fig. 24** represents different fabricated planar and 3D structures with printing speeds of 0.1-30 mm/s and nozzle diameters of 0.2-1.5 mm. **Fig. 24a** shows a matrix-like structure (composed of 6 layers), fabricated in a layer-by-layer manner while **Fig. 24b** is a filament with freeform spanning feature. **Fig. 24c** shows three similar planar structures with different optical transparency, fabricated by controlling printing parameters.

According to the authors, these 3D-printed microstructures might have potentials in optics and optofluidics[94].

4. 3D printing using nanomaterial solutions

In this section, several other interesting recent works in which nanomaterial solutions (instead of polymer nanocomposites) have been used as printing materials are briefly presented and discussed. The technique mainly used in these works is an advanced inkjet printing, called electrohydrodynamic inkjet printing (e-jetP) technique which was used for inkjet printing of nanomaterial droplets. Compared to conventional thermal or piezoelectric inkjet printing techniques, e-jetP uses an electric field for ejecting jets based on the electrohydrodynamic stability of a liquid meniscus.[95] Liquid ejection occurs when the electric stresses, induced by the electric filed overcome the effect of surface tension. The droplets are deposited on the substrate in a layer-by-layer manner and quickly dry upon fast liquid evaporation, leading to the fabrication of 3D structures. Detailed underlying process and the parameters involved in the formation of liquid cones and jets for the fabrication of 2D and 3D structures at nano- and microscale have been reviewed by Onses *et al*.[96] They also presented in details and compared different printing techniques with similar principles. E-jetP is capable of fabricating 2D and 3D structures of designed shapes and sizes in nano- and micro-scales with a very high resolution (below 100 nm).[95, 96] Due to their small size, nanomaterials can be incorporated into proper e-jet liquids without clogging the dispensing nozzle.[95]

An *et al*.[97] reported on the preparation of several ink materials containing silver, copper and cobalt nanoparticles for e-jetP of 3D structures. **Fig. 25a** represents an SEM image of e-jet printed copper pillar having a diameter of ~2 μm and a height of 20 μm. Copper nanoparticle suspension (30 wt.%) was mixed with n-tetradecane (1:1 weight ratio) to reduce the material viscosity (12.3

Pa.s) and prevent nozzle clogging. The e-jetP setup used consisted of a five-axis positioning stage, a computer-controlled power supply, a copper coated nozzle (inter diameter of 2 µm) and a pressure controller. To fabricate the copper pillar, a voltage of 400 V and a nozzle-substrate distance of 30-100 µm were used. The authors mentioned that the diameter of the pillar can be controlled by the diameter of the nozzle. The e-jetP of several other 3D structures such as a series of pillars printed close to each other, 3D walls and freestanding interconnects with their detailed printing parameters has been also presented in their work. In another work, An *et al.*[95] reported on the preparation of an ink containing rGO nanoparticles used for e-jetP of electrically conductive patterns on both flat and curved surfaces. The ink material was a mixture of rGO nanoparticles and dimethylformamide (DMF) (1 mg/mL). **Fig. 25b** shows an SEM image of the rGO alphabetic patterns printed on the sidewall of a glass capillary (nonplanar surface) using a nozzle (with a cone geometry) having an internal diameter of 5 µm and a high radius of curvature (50-65 µm). The 5-axis positioning stage used in their work enabled keeping the distance between the nozzle and the substrate constant for accurate fabrication. The authors also presented the fabrication of nonplanar patterns on the coins and other interesting devices such as an all-printed field-effect transistor.[95] Galiker *et al.*[98] demonstrated the use of gold nanoparticles solution for e-jetP of 2D and 3D nanostructures with feature sizes as low as 50 nm. The printing material was a solution of gold nanoparticles having a diameter of 3-7 nm with particle concentration of ~0.1 vol.% in a mixed solution of *n*-tetradecane and cyclododecene (50:1 wt./wt.). **Fig. 25c** shows SEM image of an e-jet printed single nanopillar with 50 nm width and 850 nm height. The printing setup was mainly composed of a 3D piezo-stage (MadCity Labs) to control the nozzle-substrate distance with nanometer accuracy, electrical equipment for pulse generation, and a microscope to observe the structure during printing. The nozzle used was a glass pipette with outer diameter of 550 nm coated with a 10 nm layer of titanium and a 100 nm layer of gold. The input voltage of up to 400V was

provided by a waveform generator (RIGOL) and a homemade HV amplifier. The authors mentioned that the e-jetP technique enabled considerable down-scaling the feature size (up to 5 times) when compared to other conventional techniques such as focused ion beam and e-beam lithography. Note that the use of other nanoparticle solutions such as silver and zinc oxide in *n*-tetradecane has been also presented in their work.

Kim *et al.*[99] presented a meniscus-guided growth approach for 3DP of freestanding reduced graphene oxide (rGO) architectures including straight wires, bridges, suspended junctions and woven structures with a fabrication accuracy of 250 nm. The printing ink material was an aqueous suspension of GO nanosheets (1 g/L) with a thickness of ~ 1 nm. **Fig. 25d** shows SEM image of a zigzag rGO nanoarch (arch width of 400 nm) printed using rGO solution. A meniscus of rGO ink was formed when the dispensing micropipette (opening diameter of 1.3 μm) was moved close enough to the substrate. The meniscus was stretched when the pipette was pulled out and the solvent (i.e., water) rapidly evaporated, enabling the fabrication of freestanding structures. This technique used a three-axis stepping motor with a positioning accuracy of 250 nm to accurately control the position of the micropipette during the 3DP. A gold-coated silicon wafer was used as substrate. All the examples discussed in this section demonstrate the capability of the e-jetP and the meniscus-guided growth 3DP techniques for the fabrication of nano- and microstructures and manufacturing of functional devices for a wide variety of applications such as microelectronics, tissue engineering, and photonics.

5. Concluding remarks, challenges and future opportunities

The integration of nanotechnology into 3DP holds great promise for manufacturing of multifunctional macro- and micro-devices by combining numerous advantages of both technologies. Significant progresses have been made over the last few years in 3DP of

nanocomposites. This paper aimed at providing the main fabrication techniques in this field with the potential applications of the 3D printed nanocomposite structures, as summarized in **Table 1**. The type of material (e.g., thermoset, thermoplastic, UV-curable) used for each technique until now and the minimum feature size that has been achieved are also indicated. **Table 2** summarizes the main process parameters, printing speed and equipment cost for all the 3DP techniques discussed in this review. A wide variety of 2D and 3D shapes with different 3D configurations (e.g., spanning, supported, and freeform) can be modeled and fabricated by using various 3DP techniques. Compared to the conventional MSL and DOPsL techniques, the extrusion-based 3DP methods offer lower cost and higher flexibility while the DOPsL seems to provide the fastest fabrication speed. It has been shown that while the nanotechnology adds functionality to the printed materials, 3DP enables the fabrication of controlled-geometry engineered structures for different applications such as components for MEMS, stretchable/flexible microelectronics, sensing devices, micro-antennas and tissue engineering.

Despite the considerable progress that has been recently made in 3DP of nanocomposites, several processing and fabrication challenges have to be still addressed. Efficient nanocomposite mixing strategies have to be used in order to minimize undesired effects of nanofillers addition on viscosity, transparency and flowability of the printing materials. The rheology of the materials is crucial in the extrusion-based 3DP technique, thus the fillers content and their dispersion can be set in order to achieve a suitable viscosity of the feedstock material for the 3DP. The MSL and DOPsL are powerful printing techniques, but they may require relatively expensive equipment when compared to some other techniques discussed in this review. The DOPsL seems the most promising technique due to its fabrication speed but it is limited to UV curable polymers. The popular FDM technique enables using high-performance spooled nanocomposite materials, but limited to relatively high minimum feature size (e.g., few hundred microns). The application of the powder-

bed technology is growing in the industry, mostly for the fabrication of metallic structures. However, the main issues associated with the powder-bed technology are the porosity of the printed product and high roughness of the printed surface, which limited the diverse utilization of this technique for 3DP of micro- and macrostructures.

To this end, it would be important to find out which type of materials and techniques are compatible. On the materials side, the development of novel materials with high level of flowability is a key factor for the further progress in the field. A diverse range of nanofillers such as nanobiomaterials, carbon nanotubes, graphene, nanoclay, metallic nanoparticles and nanowires and also host materials (e.g., thermoplastics and thermosets) can be adapted for 3DP of multifunctional materials. Although the polymers are the most commonly used printing materials so far, other types of materials such as liquid metals can be also used.[6] On the fabrication side, the evolution of high precision robots or moving stages is another key factor for the further improvement of the resolution of the manufactured structures. In addition, the capability of other existing fabrication techniques for 3DP of nanocomposites should be examined while looking into the development of new 3DP approaches. It would be interesting to design machines with multifunctional printing capability and to combine different 3DP techniques. The parallel advances on both sides will lead to the development of miniaturized functional devices with 3D shape optimization for a wide range of applications.

References

[1]   M. Cima, E. Sachs, L. Cima, J. Yoo, S. Khanuja, S. Borland, B. Wu, R. Giordano, "Computer-derived microstructures by 3D printing: bio-and structural materials", presented at *Solid Freeform Fabr. Symp. Proc*, 1994.

[2]   B. Utela, D. Storti, R. Anderson, M. Ganter, Journal of Manufacturing Processes 2008, 10, 96.

[3]   K. Leong, C. Cheah, C. Chua, Biomaterials 2003, 24, 2363.

[4]   http://www.designboom.com/technology/nanoscribe-nanoscale-3d-printed-microstructures/ 2013.

[5]   a) R. Engelke, G. Engelmann, G. Gruetzner, M. Heinrich, M. Kubenz, H. Mischke, Microelectronic engineering 2004, 73, 456; b) J. D. Pitts, P. J. Campagnola, G. A. Epling, S. L. Goodman, Macromolecules 2000, 33, 1514.

[6]   C. Ladd, J. H. So, J. Muth, M. D. Dickey, Advanced Materials 2013, 25, 5081.

[7]   M. Feldmann, A. Waldschik, S. Büttgenbach, "Electromagnetic micro-actuators, micro-motors, and micro-robots", presented at *Microelectronics, MEMS, and Nanotechnology*, 2007.

[8]   A. Yamada, F. Niikura, K. Ikuta, Journal of Micromechanics and Microengineering 2008, 18, 025035.

[9]   S. Z. Guo, F. Gosselin, N. Guerin, A. M. Lanouette, M. C. Heuzey, D. Therriault, Small 2013, 9, 4118.

[10]   L. L. Lebel, B. Aissa, M. A. E. Khakani, D. Therriault, Advanced materials 2010, 22, 592.

[11]   J. J. Adams, E. B. Duoss, T. F. Malkowski, M. J. Motala, B. Y. Ahn, R. G. Nuzzo, J. T. Bernhard, J. A. Lewis, Advanced Materials 2011, 23, 1335.

[12]   S.-z. Guo, X. Yang, M.-C. Heuzey, D. Therriault, Nanoscale 2015, 7, 6451.

[13]   Y. L. Kong, I. A. Tamargo, H. Kim, B. N. Johnson, M. K. Gupta, T.-W. Koh, H.-A. Chin, D. A. Steingart, B. P. Rand, M. C. McAlpine, Nano letters 2014, 14, 7017.

[14]   W. Chee, H. Lim, N. Huang, I. Harrison, RSC Advances 2015, 5, 68014.

[15]   B. G. Compton, J. A. Lewis, Advanced Materials 2014, 26, 5930.

[16]   R. D. Farahani, H. Dalir, V. Le Borgne, L. A. Gautier, M. A. El Khakani, M. Lévesque, D. Therriault, Composites Science and Technology 2012, 72, 1387.

[17]   R. D. Farahani, H. Dalir, V. Le Borgne, L. A. Gautier, M. A. El Khakani, M. Lévesque, D. Therriault, Nanotechnology 2012, 23, 085502.

[18]   A. Frutiger, J. T. Muth, D. M. Vogt, Y. Mengüç, A. Campo, A. D. Valentine, C. J. Walsh, J. A. Lewis, Advanced Materials 2015, 27, 2440.

[19]   T. Wu, Y. Pan, E. Liu, L. Li, Journal of Applied Polymer Science 2012, 126, E283.

[20]   S. J. Leigh, C. Purssell, J. Bowen, D. A. Hutchins, J. A. Covington, D. Billson, Sensors and Actuators A: Physical 2011, 168, 66.

[21]   A. Patole, I. A. Ventura, G. Lubineau, Journal of Applied Polymer Science 2015, 132.

[22]   X. Peng, F. Tan, W. Wang, X. Qiu, F. Sun, X. Qiao, J. Chen, Journal of Materials Science: Materials in Electronics 2014, 25, 1149.

[23]   M. H. Al-Saleh, G. A. Gelves, U. Sundararaj, Composites Part A: Applied Science and Manufacturing 2011, 42, 92.

[24]   H. Kishi, S. Tanaka, Y. Nakashima.

[25]   a) T. M. Kruckenberg, V. A. Hill, A. M. Mazany, E. Young, S. Chiou, Google Patents, 2015; b) J. Sumfleth, X. C. Adroher, K. Schulte, Journal of materials science 2009, 44, 3241.

[26]   a) J. Gou, Y. Tang, F. Liang, Z. Zhao, D. Firsich, J. Fielding, Composites Part B: Engineering 2010, 41, 192; b) J. Zhu, S. Wei, J. Ryu, M. Budhathoki, G. Liang, Z. Guo, Journal of Materials Chemistry 2010, 20, 4937.

[27]   J. Zhu, M. Chen, Q. He, L. Shao, S. Wei, Z. Guo, Rsc Advances 2013, 3, 22790.

[28]   T. D. Fornes, N. D. Huffman, S. B. Carruthers, "Eliminating tradeoffs in conductive composites via novel heterogeneous structures", presented at *2009 SAMPE Fall Technical Conference and Exhibition-Global Material Technology: Soaring to New Horizons*, 2009.

[29]   a) H. Murakami, T. Nomura, N. Nakashima, Chemical Physics Letters 2003, 378, 481; b) L. Sun, G. Warren, J. O'reilly, W. Everett, S. Lee, D. Davis, D. Lagoudas, H.-J. Sue, Carbon 2008, 46, 320.

[30]   N. Minami, Y. Kim, K. Miyashita, S. Kazaoui, B. Nalini, Applied Physics Letters 2006, 88, 093123.

[31]   R. D. Farahani, M. Pahlavanpour, H. Dalir, B. Aissa, M. A. El Khakani, M. Lévesque, D. Therriault, Materials & Design 2012, 41, 214.

[32]   L. L. Lebel, B. Aissa, M. A. El Khakani, D. Therriault, Composites Science and Technology 2010, 70, 518.

[33]   R. D. Farahani, H. Dalir, B. Aissa, M. A. El Khakani, M. Lévesque, D. Therriault, Composites Part A: Applied Science and Manufacturing 2011, 42, 1910.

[34]   M. Moniruzzaman, F. Du, N. Romero, K. I. Winey, Polymer 2006, 47, 293.

[35]   S. Wang, R. Liang, B. Wang, C. Zhang, Nanotechnology 2008, 19, 085710.

[36]   R. D. Farahani, J. E. Klemberg-Sapieha, D. Therriault, Materials & Design 2015, 88, 1175.

[37]   J. N. Coleman, U. Khan, Y. K. Gun'ko, Advanced Materials 2006, 18, 689.

[38]   M. Rong, M. Zhang, W. Ruan, Materials science and technology 2006, 22, 787.

[39]   S. Abbasi, P. J. Carreau, A. Derdouri, Polymer 2010, 51, 922.

[40]   E. T. Thostenson, T.-W. Chou, Carbon 2006, 44, 3022.

[41]   S.-Z. Guo, M.-C. Heuzey, D. Therriault, Langmuir 2014, 30, 1142.

[42]   R. Passieux, L. Guthrie, S. H. Rad, M. Lévesque, D. Therriault, F. P. Gosselin, Advanced Materials 2015, 27, 3708.

[43]   a) A. Alateyah, H. Dhakal, Z. Zhang, Advances in Polymer Technology 2013, 32; b) F. Hussain, M. Hojjati, M. Okamoto, R. E. Gorga, Journal of composite materials 2006, 40, 1511; c) J. Wei, T. Vo, F. Inam, RSC Advances 2015, 5, 73510.

[44]   D. Yugang, Z. Yuan, T. Yiping, L. Dichen, Rapid Prototyping Journal 2011, 17, 247.

[45]   R. Goodridge, M. Shofner, R. Hague, M. McClelland, M. Schlea, R. Johnson, C. Tuck, Polymer Testing 2011, 30, 94.

[46]   K. Chizari, D. Therriault, "Fabrication of Conductive Microfilaments and Liquid Sensor from CNTs/PLA Nanocomposites", presented at *Design, Manufacturing and Applications of Composites Tenth Workshop 2014: Proceedings of the Tenth Joint Canada-Japan Workshop on Composites, August 2014, Vancouver, Canada*, 2015.

[47]   C.-X. Liu, J.-W. Choi, Journal of Micromechanics and Microengineering 2009, 19, 085019.

[48]   X. C. Wu, A. M. Bittner, K. Kern, Advanced Materials 2004, 16, 413.

[49]   A. Chiolerio, I. Roppolo, M. Sangermano, RSC Advances 2013, 3, 3446.

[50]   http://www.eps.manchester.ac.uk/our-research/research-facilities/digital-fabrication/about-us/about-printing/.

[51]   M. Vaezi, H. Seitz, S. Yang, The International Journal of Advanced Manufacturing Technology 2013, 67, 1721.

[52]   G. Wang, Z. Wang, Z. Liu, J. Xue, G. Xin, Q. Yu, J. Lian, M. Y. Chen, Chemical Engineering Journal 2015, 260, 582.

[53]   K. Chi, Z. Zhang, J. Xi, Y. Huang, F. Xiao, S. Wang, Y. Liu, ACS applied materials & interfaces 2014, 6, 16312.

[54]   A. M. Elliott, O. S. Ivanova, C. B. Williams, T. A. Campbell, Advanced Engineering Materials 2013, 15, 903.

[55]   http://www.custompartnet.com/wu/3d-printing.

[56]   J. A. Lewis, G. M. Gratson, Materials today 2004, 7, 32.

[57]   J. Czyżewski, P. Burzyński, K. Gaweł, J. Meisner, Journal of Materials Processing Technology 2009, 209, 5281.

[58]   A. Azhari, E. Toyserkani, C. Villain, International Journal of Applied Ceramic Technology 2015, 12, 8.

[59]   S. Kawata, H.-B. Sun, T. Tanaka, K. Takada, Nature 2001, 412, 697.

[60]   J. Fischer, M. Wegener, Laser & Photonics Reviews 2013, 7, 22.

[61]   J. K. Hohmann, M. Renner, E. H. Waller, G. von Freymann, Advanced Optical Materials 2015, 3, 1488.

[62]   X. Zhou, Y. Hou, J. Lin, AIP Advances 2015, 5, 030701.

[63]   Q. Guo, R. Ghadiri, S. Xiao, C. Esen, O. Medenbach, A. Ostendorf, "Laser direct writing of high refractive index polymer/TiO2 nanocomposites", presented at *SPIE LASE*, 2012.

[64]   A. P. Zhang, X. Qu, P. Soman, K. C. Hribar, J. W. Lee, S. Chen, S. He, Advanced Materials 2012, 24, 4266.

[65]   M. P. Lee, G. J. Cooper, T. Hinkley, G. M. Gibson, M. J. Padgett, L. Cronin, Scientific reports 2015, 5, 9875.

[66]   M. Gou, X. Qu, W. Zhu, M. Xiang, J. Yang, K. Zhang, Y. Wei, S. Chen, Nature communications 2014, 5.

[67]   D. Therriault, R. F. Shepherd, S. R. White, J. A. Lewis, Advanced Materials 2005, 17, 395.

[68]   D. Therriault, S. R. White, J. A. Lewis, Nature materials 2003, 2, 265.

[69]   D. Therriault, S. R. White, J. A. Lewis, Applied Rheology 2007, 17, 10112.

[70]   R. Farahani, L. Lebel, D. Therriault, Journal of Micromechanics and Microengineering 2014, 24, 055020.

[71]   R. D. Farahani, K. Chizari, D. Therriault, Nanoscale 2014, 6, 10470.

[72]   a) G. M. Gratson, J. A. Lewis, Langmuir 2005, 21, 457; b) G. M. Gratson, M. Xu, J. A. Lewis, Nature 2004, 428, 386; c) J. E. Smay, G. M. Gratson, R. F. Shepherd, J. Cesarano, J. A. Lewis, Advanced Materials 2002, 14, 1279.

[73]   B. Y. Ahn, S. B. Walker, S. C. Slimmer, A. Russo, A. Gupta, S. Kranz, E. B. Duoss, T. F. Malkowski, J. A. Lewis, Journal of visualized experiments: JoVE 2011, 58, e3189.

[74]   R. Dermanaki-Farahani, L. L. Lebel, D. Therriault, Journal of visualized experiments: JoVE 2014, 85, e51512.

[75]   B. Aïssa, E. Haddad, W. Jamroz, S. Hassani, R. Farahani, P. Merle, D. Therriault, Smart Materials and Structures 2012, 21, 105028.

[76]   C. J. Hansen, S. R. White, N. R. Sottos, J. A. Lewis, Advanced Functional Materials 2011, 21, 4320.

[77]   A. Tsouknidas, Advances in Tribology 2011, 746270.

[78]   a) M. Allahverdi, S. Danforth, M. Jafari, A. Safari, Journal of the European Ceramic Society 2001, 21, 1485; b) J. Mireles, D. Espalin, D. Roberson, B. Zinniel, F. Medina, R. Wicker, 2013; A. Safari, Ferroelectrics 2001, 263, 45.

[79]   a) S. Kumar, J.-P. Kruth, Materials & Design 2010, 31, 850; b) C. Lee, S. Kim, H. Kim, S. Ahn, Journal of materials processing technology 2007, 187, 627; c) M. McGurk, A. Amis, P.

Potamianos, N. Goodger, Annals of the Royal College of Surgeons of England 1997, 79, 169; d) J. E. Rabinovich, Google Patents, 1996, US5578227.

[80]   N. J. Castro, R. Patel, L. G. Zhang, Cellular and Molecular Bioengineering, 2015, 8, 416.

[81]   M. Bouchaar, École Polytechnique de Montréal, Master Thesis, 2011, 544.

[82]   S. Ahmadi, P. Nassiri, I. Ghasemi, M. R. M. Ep, Global Journal of Health Science 2015, 8, 180.

[83]   S. J. Leigh, R. J. Bradley, C. P. Purssell, D. R. Billson, D. A. Hutchins, 2012, PLoS ONE 7(11): e49365.

[84]   G. Postiglione, G. Natale, G. Griffini, M. Levi, S. Turri, Composites Part A: Applied Science and Manufacturing 2015, 76, 110.

[85]   N. Guérin, M. Lévesque, D. Therriault, Journal of Biomedical Science and Engineering 2014, 7, 641.

[86]   B. Y. Ahn, E. B. Duoss, M. J. Motala, X. Guo, S.-I. Park, Y. Xiong, J. Yoon, R. G. Nuzzo, J. A. Rogers, J. A. Lewis, Science 2009, 323, 1590.

[87]   M. Vatani, E. D. Engeberg, J.-W. Choi, Additive Manufacturing 2014, 7, 73.

[88]   C. Decker, Progress in polymer science 1996, 21, 593.

[89]   N. Hu, Y. Karube, C. Yan, Z. Masuda, H. Fukunaga, Acta Materialia 2008, 56, 2929.

[90]   B. Wang, J. Zheng, Y. He, Q. Sheng, Sensors and Actuators B: Chemical 2013, 186, 417.

[91]   H. Cao, Z. Gan, Q. Lv, H. Yan, X. Luo, X. Song, S. Liu, Microsystem Technologies 2010, 16, 955.

[92]   L. Laberge Lebel, École Polytechnique de Montréal, Ph.D Thesis 2009, 70-12, 7808.

[93]   B. Aïssa, D. Therriault, R. Farahani, L. Lebel, M. El Khakani, Nanotechnology 2012, 23, 115705.

[94]   G. Postiglione, G. Natale, G. Griffini, M. Levi, S. Turri, Polymer Composites 2015, DOI: 10.1002/pc.23735.

[95]   B. W. An, K. Kim, M. Kim, S. Y. Kim, S. H. Hur, J. U. Park, Small 2015, 11, 2263.

[96]   M. S. Onses, E. Sutanto, P. M. Ferreira, A. G. Alleyne, J. A. Rogers, small 2015, 11, 4237.

[97]   B. W. An, K. Kim, H. Lee, S. Y. Kim, Y. Shim, D. Y. Lee, J. Y. Song, J. U. Park, Advanced Materials 2015, 27, 4322.

[98]   P. Galliker, J. Schneider, H. Eghlidi, S. Kress, V. Sandoghdar, D. Poulikakos, Nature communications 2012, 3, 890.

[99]   J. H. Kim, W. S. Chang, D. Kim, J. R. Yang, J. T. Han, G. W. Lee, J. T. Kim, S. K. Seol, Advanced Materials 2015, 27, 157.

[100]   A. Chiolerio, V. Camarchia, R. Quaglia, M. Pirola, P. Pandolfi, C. F. Pirri, Journal of Alloys and Compounds 2014, 615, S501.

[101]   R. Giardi, S. Porro, A. Chiolerio, E. Celasco, M. Sangermano, Journal of Materials Science 2013, 48, 1249.

Figures and Tables
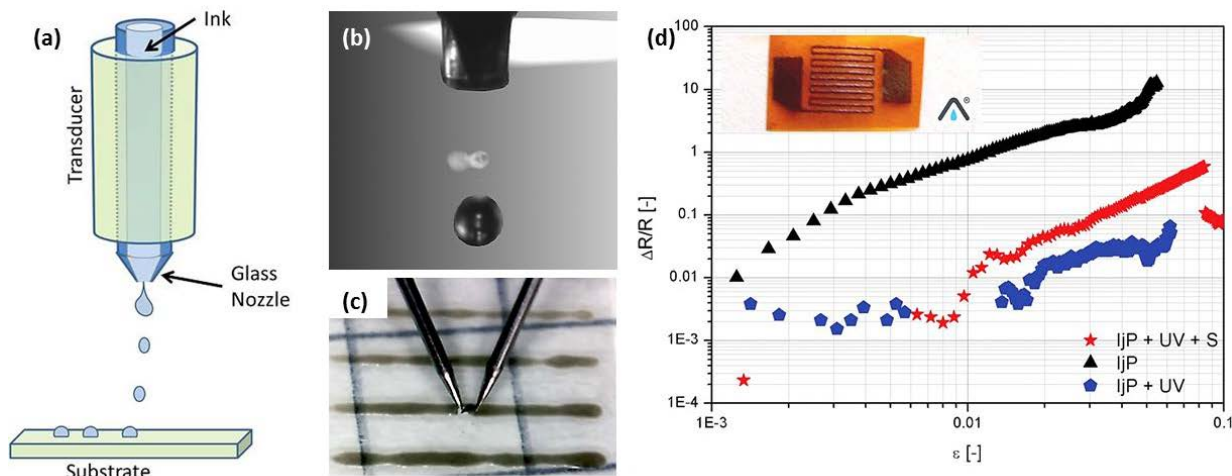
Fig. 1. (a) Schematic illustration of a piezoelectric drop-on-demand inkjet printing method,[50] (b) image of an ink droplet of silver nitrate solution,[100] (c) photo of deposited filaments made of graphene oxide filled PEGDA nanocomposites during electrical resistivity measurement,[101] and (d) piezoresistivity curves of strain gauges made of silver precursors (AgSbF$_6$, 30 wt.%) and titanium (TiO$_2$, 5 wt.%) nanoparticles mixed with a photocurable resin.[49]
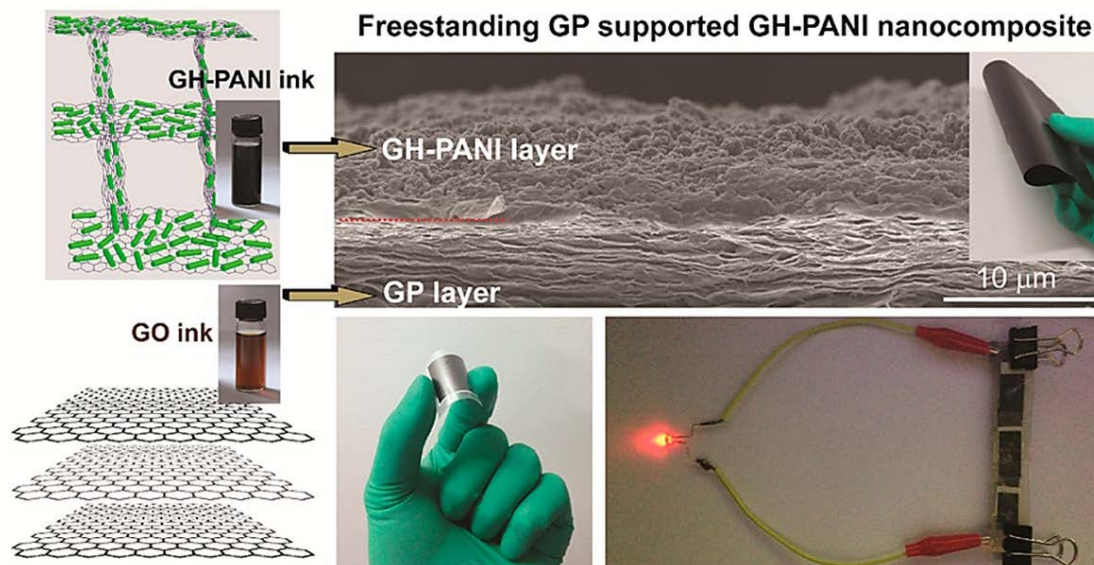
Fig. 2. Flexible all-solid-state supercapacitor device fabricated by the inkjet printing. A 3D porous graphene hydrogel nanocomposite is supported by a freestanding graphene paper.[53]
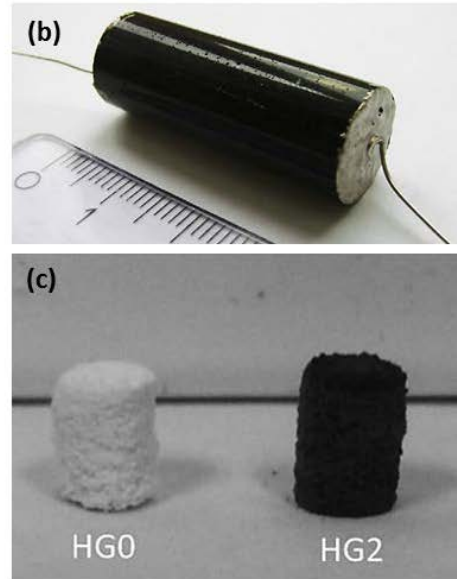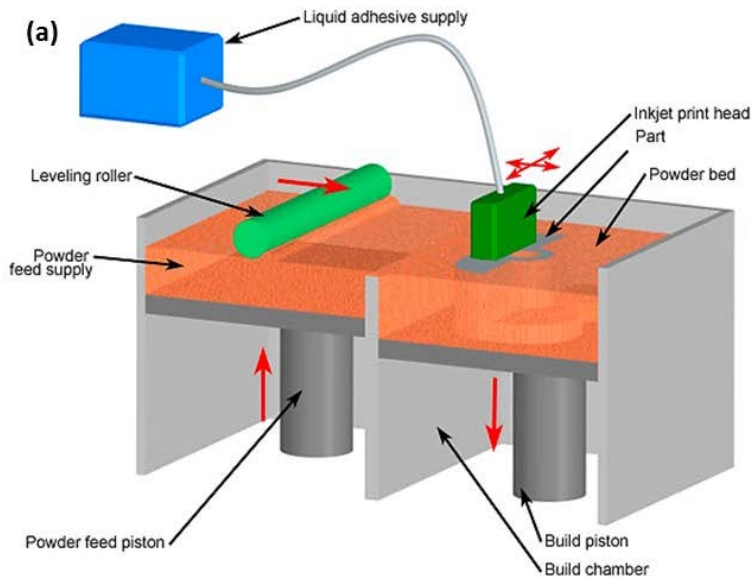
Fig. 3. (a) Schematic illustration of a layer-by-layer fabrication of a 3D structure using the powder bed technology,[55] (b) photo of printed carbon nanofiber nanocomposite sample prepared for volume electrical measurements,[57] and (c) porous structures (cylinders) of nanocomposites containing 0 wt.% GO (HG0) and 0.2 wt.% GO (HG2) fabricated by powder-bed 3DP.[58]
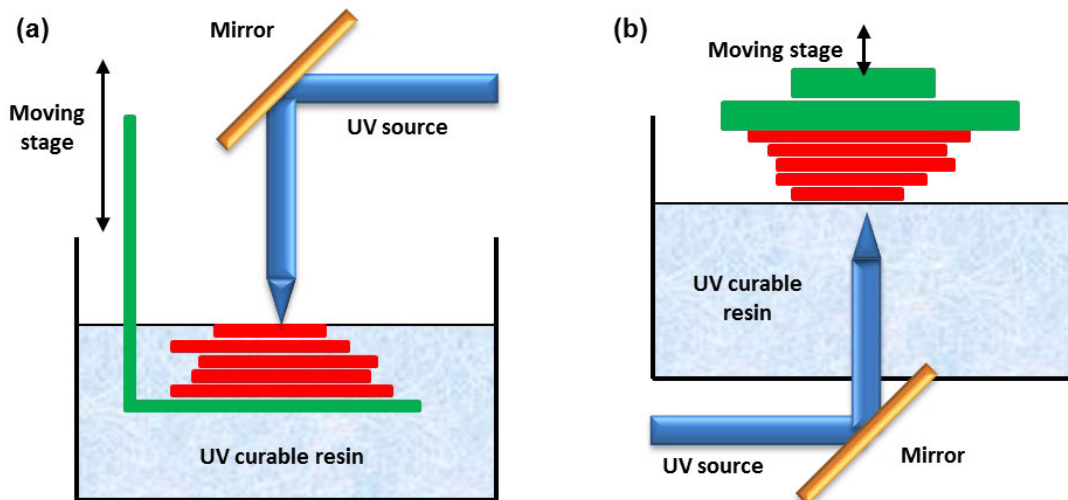
Fig. 4. Schematic representation of a layer-by-layer fabrication of a 3D structure using the MSL technique in classic (a) and inverted (b) configurations.
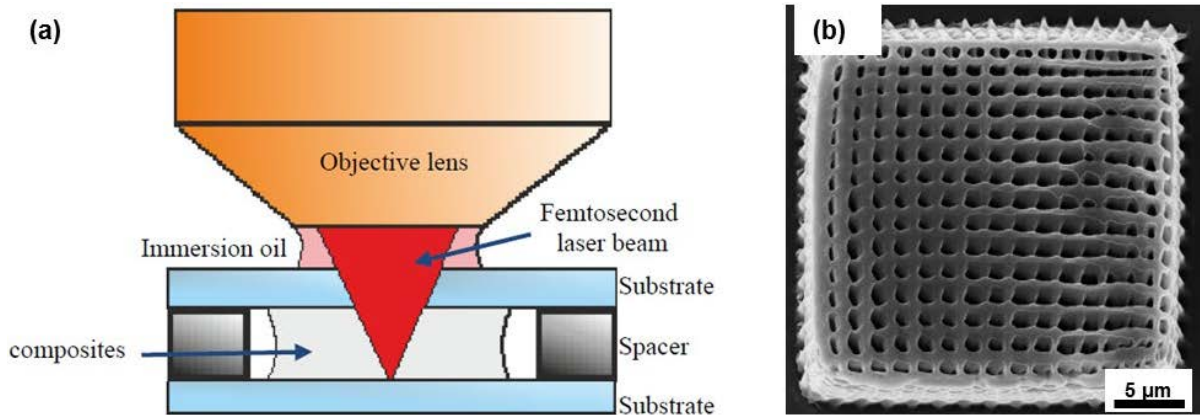
Fig. 5. (a) Schematic representation of laser direct fabrication principle of 3D periodic scaffold structures and (b) SEM image of a fabricated structure using 1 wt.% TiO_2 *sol*, 0.1048% TiO_2 nanoparticles.[63]
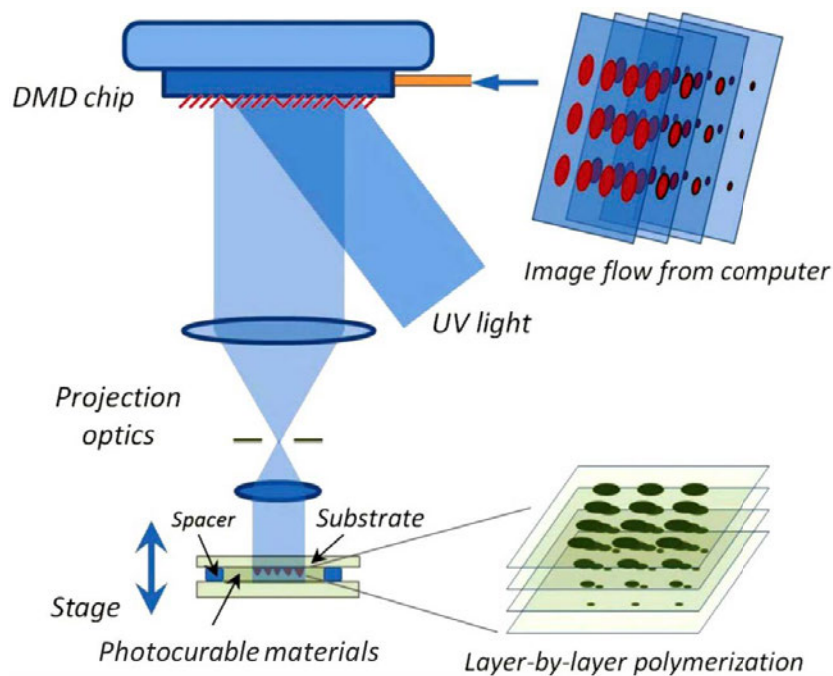
Fig. 6. Schematic representation of a complex 3D pattern using the DOPsL technique. The structure is fabricated layer by layer using dynamic virtual photomasks produced by a digital mirror array device (DMD).[64]
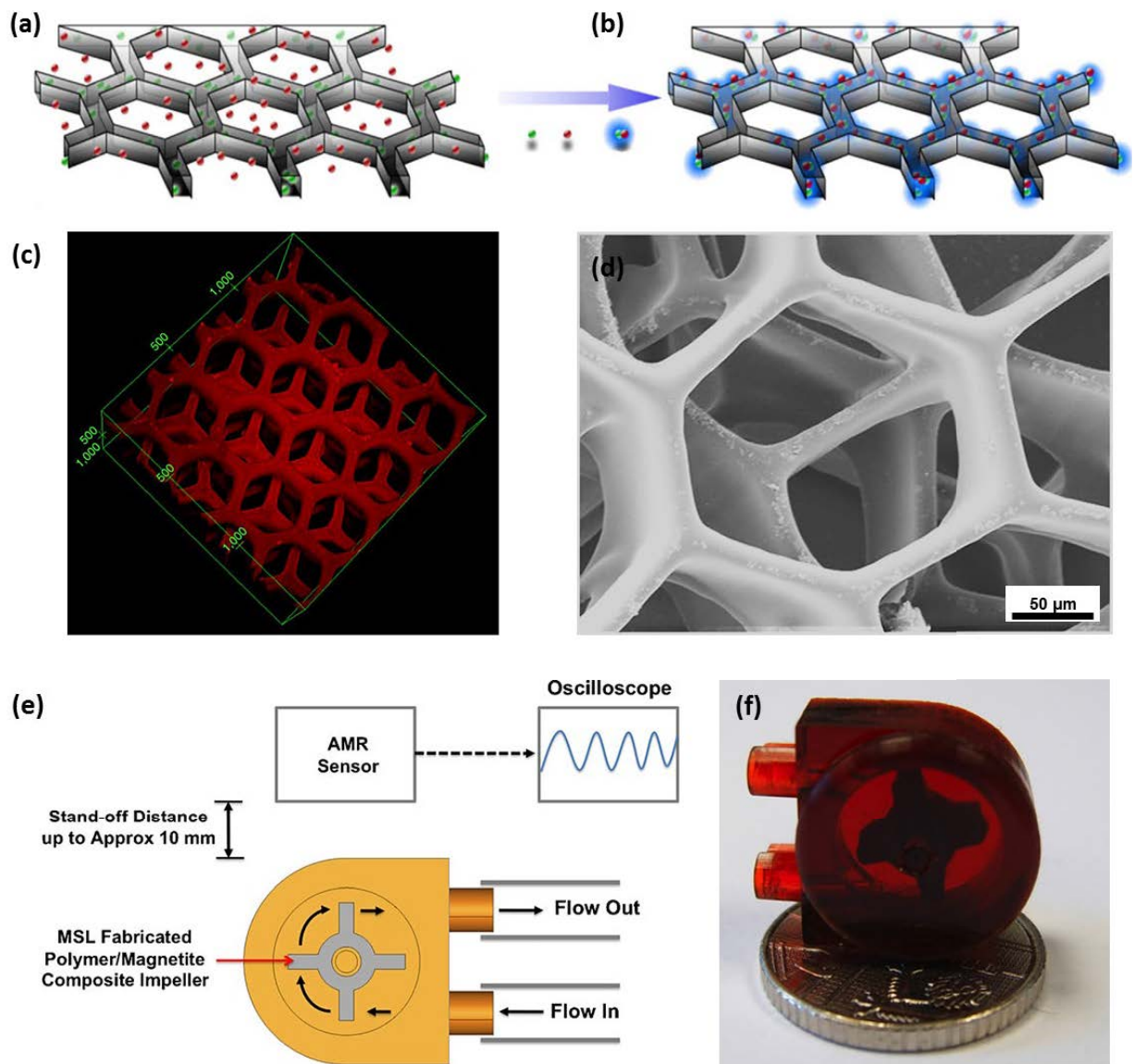
Fig. 7. Scheme of (a) a liver mimetic structure with PDA nanoparticles (green) fabricated by DOPsL 3DP technique, (b) toxins (red) captured by the nanoparticles, (c) laser confocal microscopy image and (d) SEM image of the 3D biomimetic device,[66] (e) schematic illustration of a flow sensor device fabricated using the DOPsL technique. The 3D printed impeller was made of a magnetic acrylic nanocomposite containing 25 wt.% of Fe_2O_3 nanoparticles, and (f) photo of the fabricated device.[20]
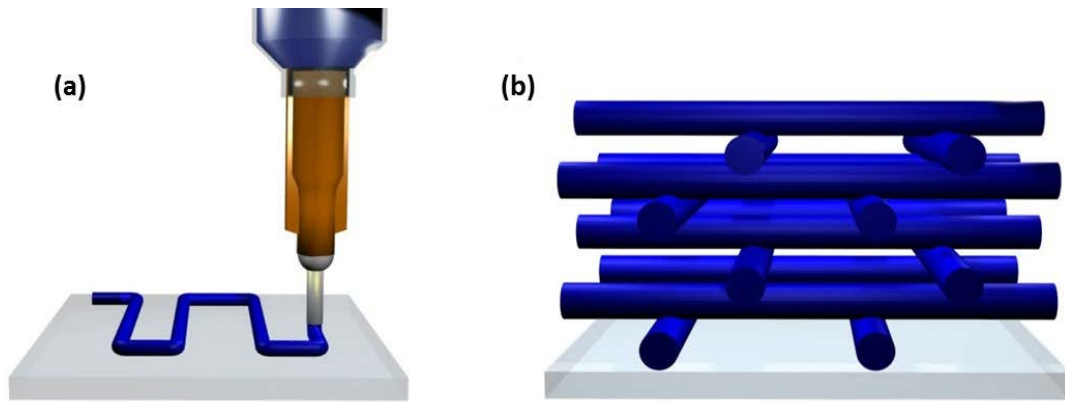
Fig. 8. Schematic illustration of the extrusion-based 3DP methods: (a) deposition of the material on a substrate to make the first 2D layer and (b) 3D periodic scaffold fabricated in layer-by-layer fashion by moving the extrusion nozzle in *z*-direction to deposit the following layers.[67]
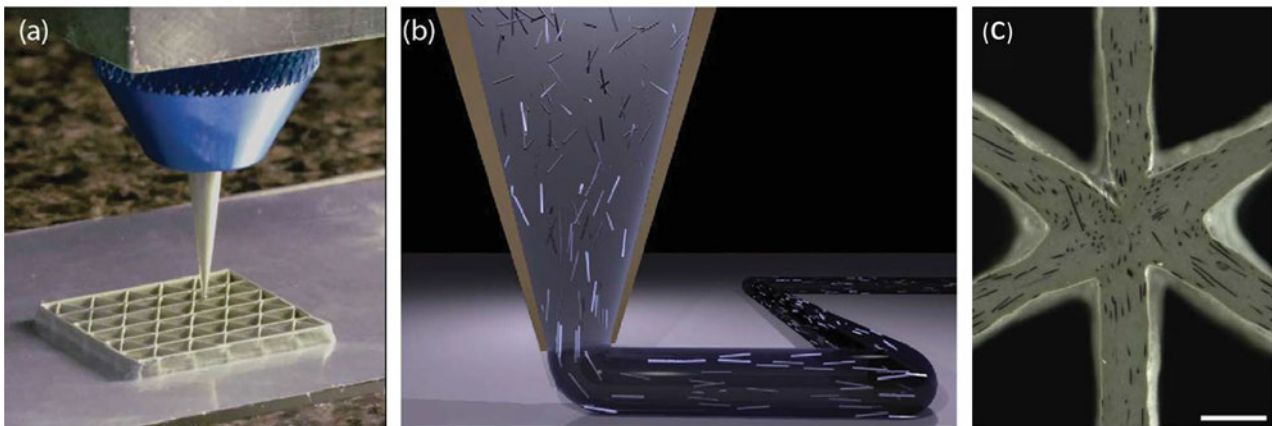
Fig. 9. (a) Optical image of a 3D printed cellular composite (b) schematic representation of the fillers' alignment material deposition, and (c) optical image of a triangular honeycomb structure showing fillers' orientation. The scale bar in (c) is 500 µm.[15]
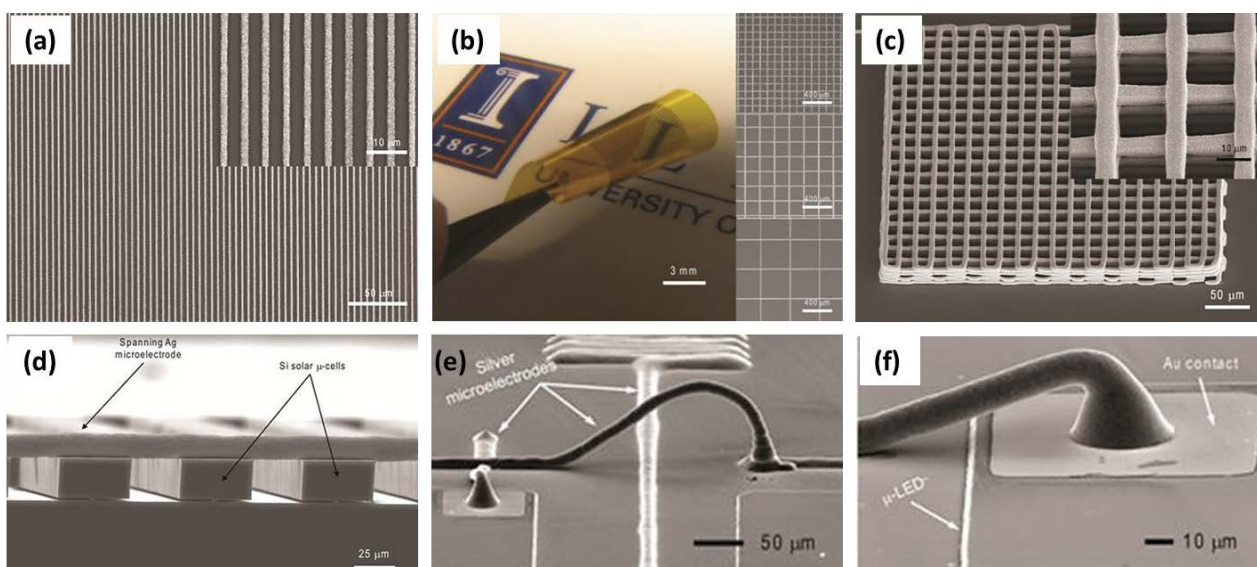
Fig. 10. Direct printing of planar and 3D patterns using conductive nanocomposite inks containing silver nanoparticles: (a) SEM images of a 2D line network, (b) optical image of conductive silver grids (left) and SEM images of some printed grids (right), (c) SEM images of periodic scaffold, and (d-f) spanning conductive interconnects for the application in photovoltaics and LEDs.[73]
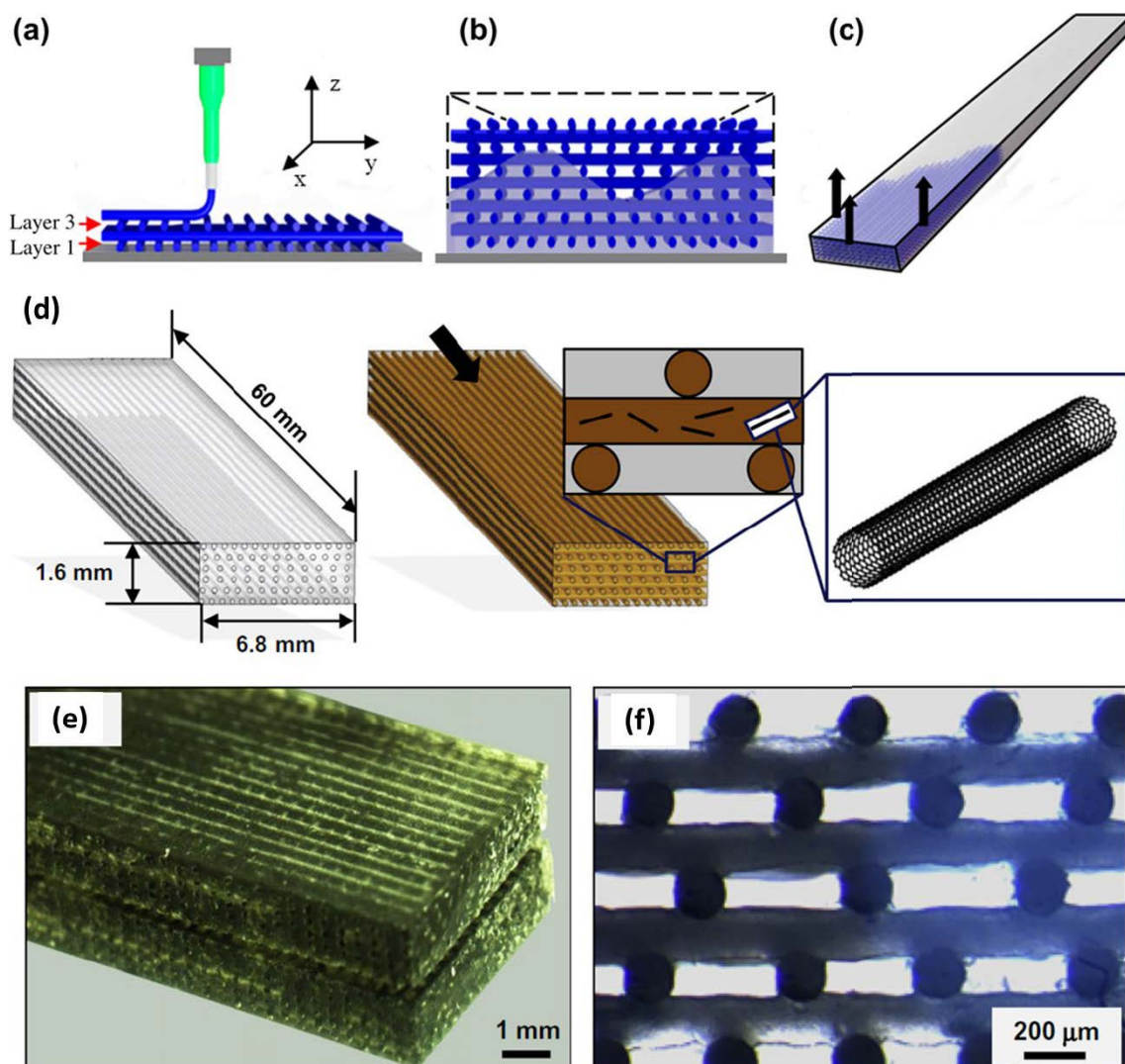
Fig. 11. Schematic representation of the manufacturing process of a 3D-reinforced nanocomposite structure through micro-infiltration of 3D microfluidic network: (a) deposition of fugitive ink scaffold on an epoxy substrate, (b) encapsulation of the 3D ink-based scaffold using epoxy resin followed by resin solidification, (c) ink removal, (d) illustration of the infiltration process using nanocomposites with overall dimensions of the microfluidic network, (e) isometric image of a 3D-reinforced beam and (d) typical cross-section of a nanocomposite structure.[31, 33]
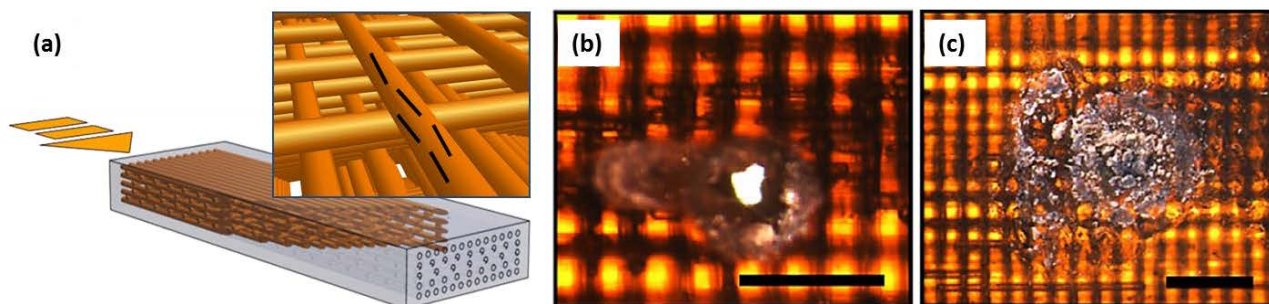
Fig. 12. (a) Infiltration of nanocomposite self-healing material into the microfluidic network, (b) and (c) optical top-view images of a microfluidic-based structure filled with nanocomposite right after the impact event and after 30 min, respectively. The scale bar is 2 mm.[75]
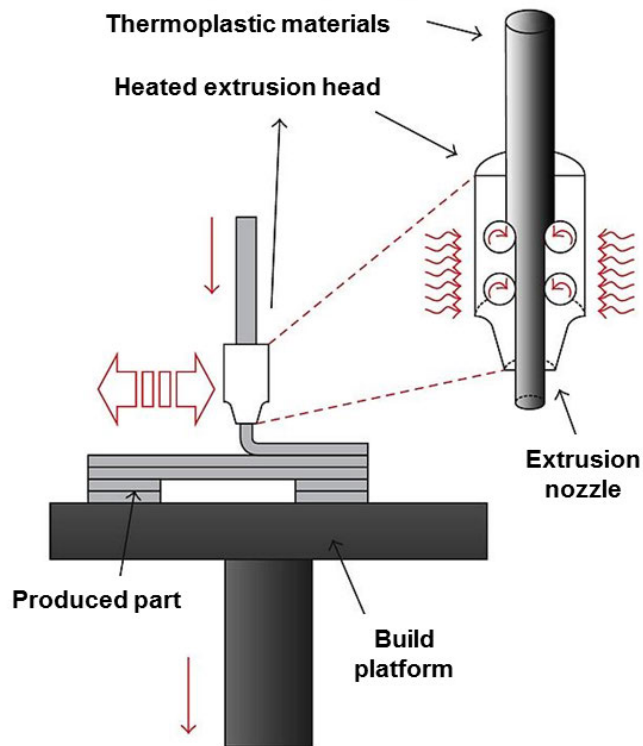
Fig. 13. Schematic illustration of the FDM method.[77]
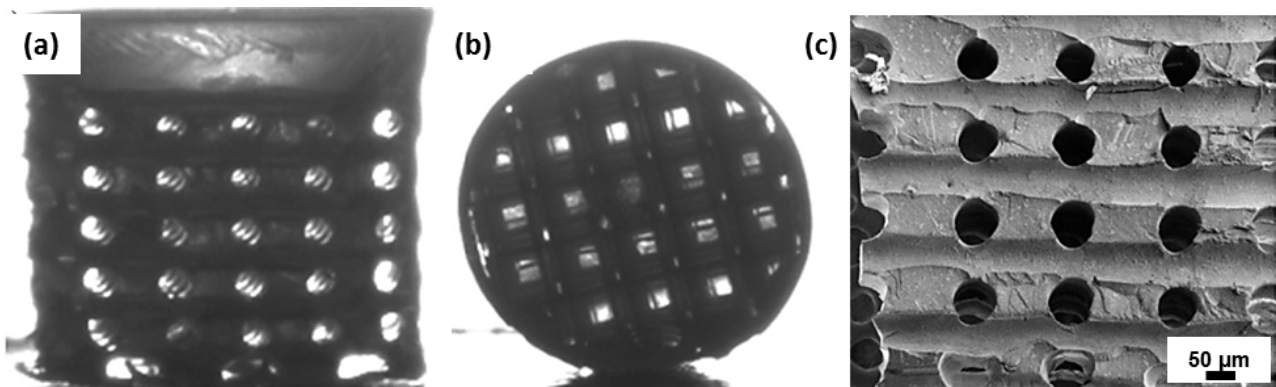
Fig. 14. (a) Side view and (b) top view optical micrograph of cylindrical polystyrene scaffold, and (c) a representative SEM image of the osteochondral scaffold illustrating horizontal and vertical channels.[80]
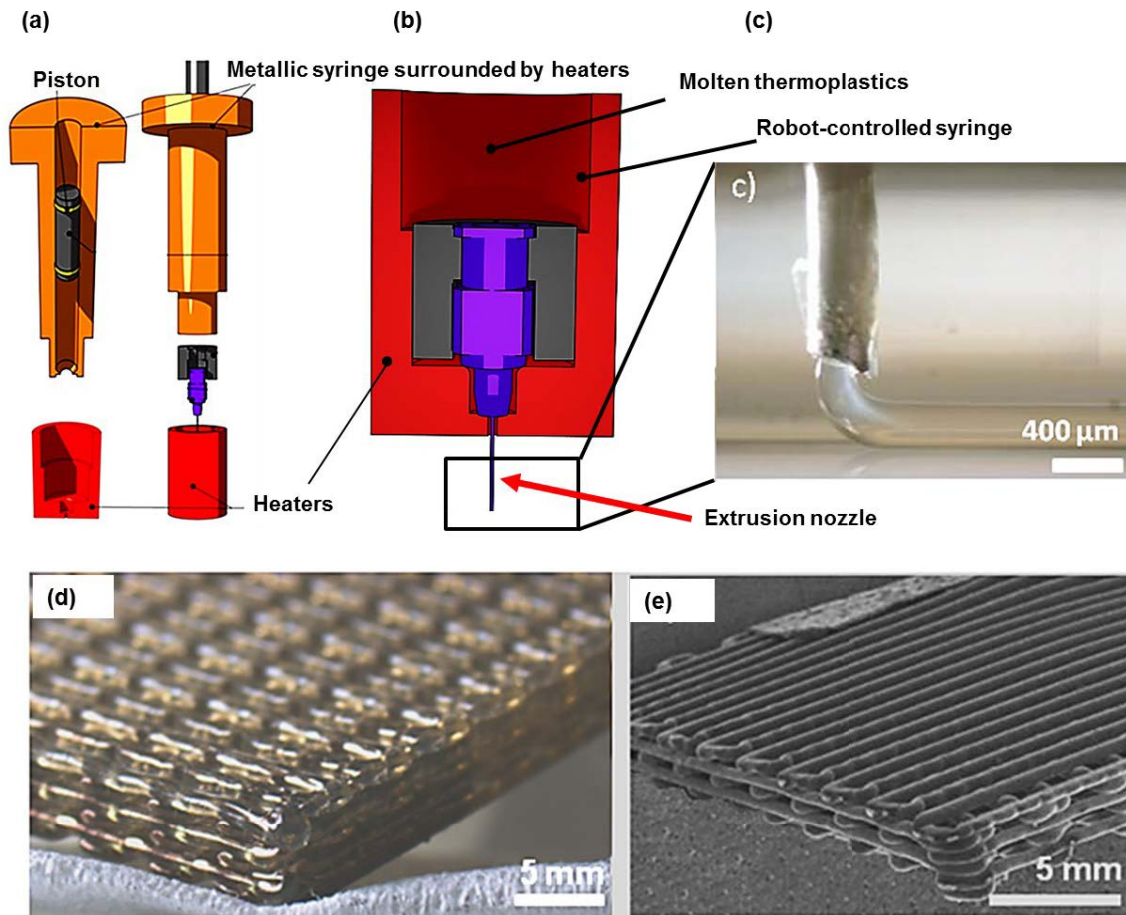
Fig. 15. (a) and (b) schematic representation of the HA-3DP method, showing the custom-made metallic syringe enclosed by the heating elements and the pressure piston, (c) optical image of an extrusion nozzle during the filament deposition, (d) optical and (e) SEM micrographs of a 6-layer 3D scaffold fabricated using PLA nanocomposites containing 2 wt.% of nanoclay by means of the HA-3DP method.[81]
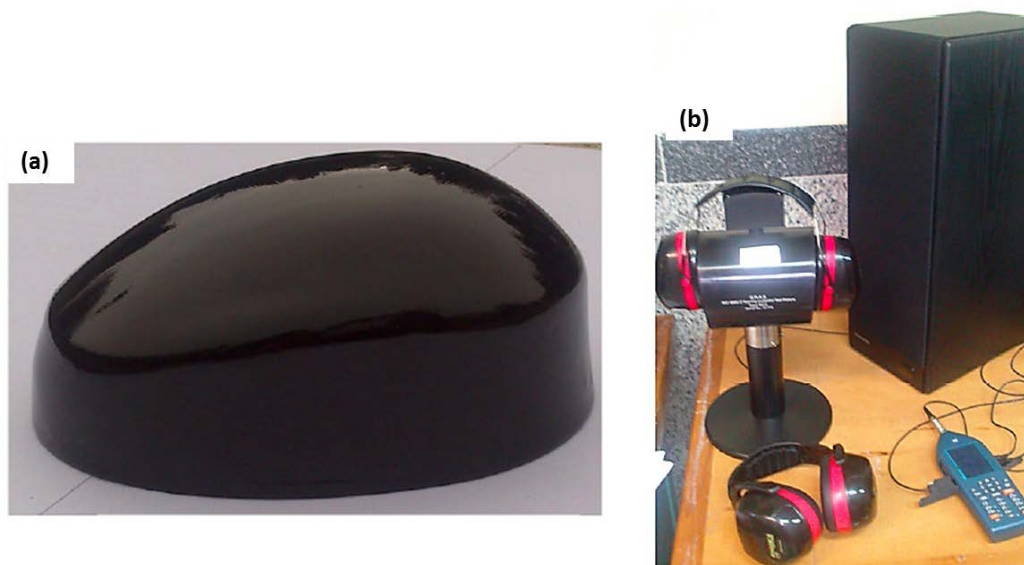
Fig. 16. Optical images of (a) a 3D printed earmuff and (b) acoustic test fixture measurement system.[82]
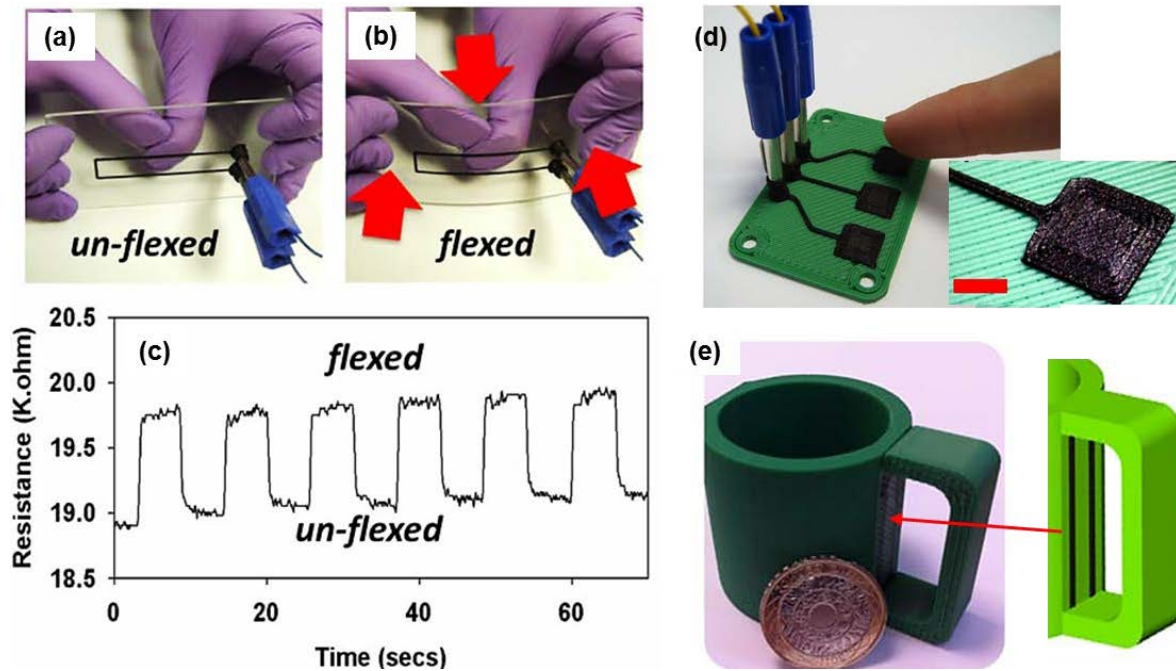
Fig. 17. Representative functional devices fabricated by the FDM technique using a carbon black/PCL nanocomposite material: (a-c) optical images and the resistance changes of a printed flex sensor in un-flexed and flexed status (the device was composed of a printed 2D nanocomposite filament), (d) photo of printed capacitive buttons with connected circuit plugs, and (e) photo of a smart printed mug containing two conductive tracks in the sides of the mug (black lines in the schematic), capable of sensing the liquid volume when being filled with water.[83]
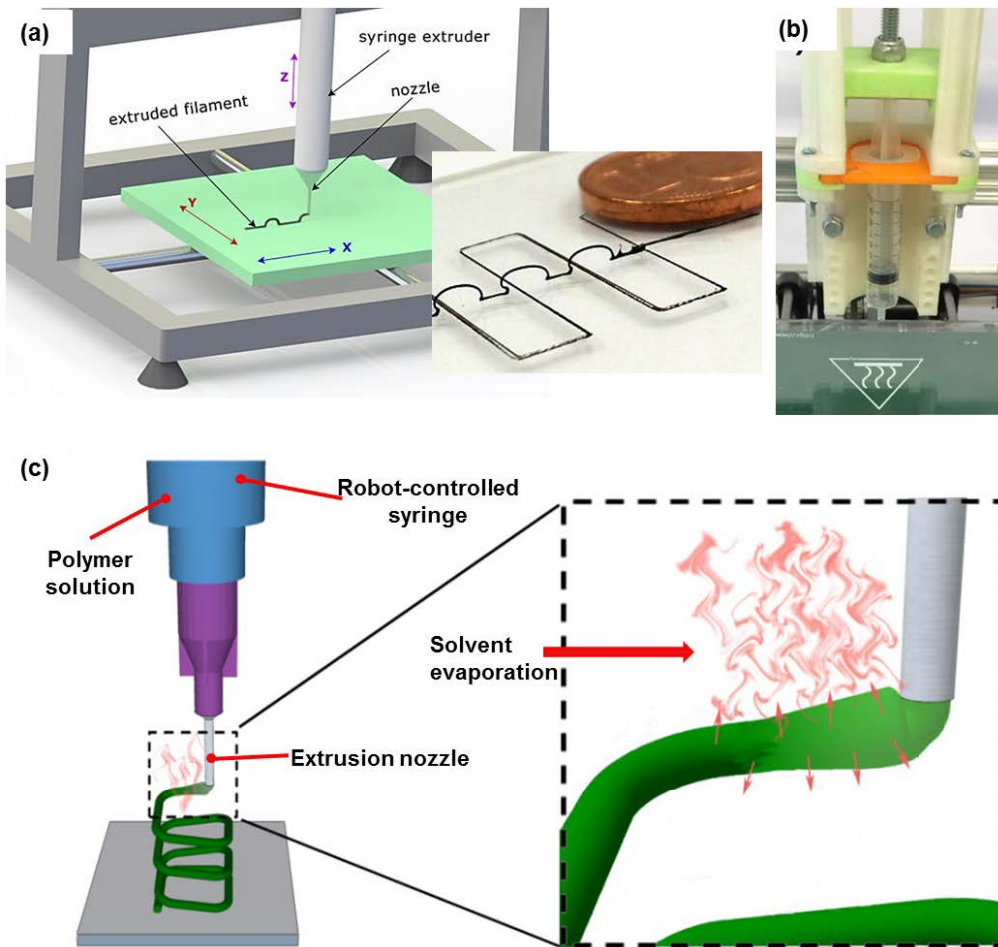
Fig. 18. (a) A scheme of the LDM process and (b) a photo of the dispensing syringe mounted onto the 3D printer header, and (c) schematic representation of SC-3DP of a 3D freeform rectangular spiral microstructure.[12, 84]
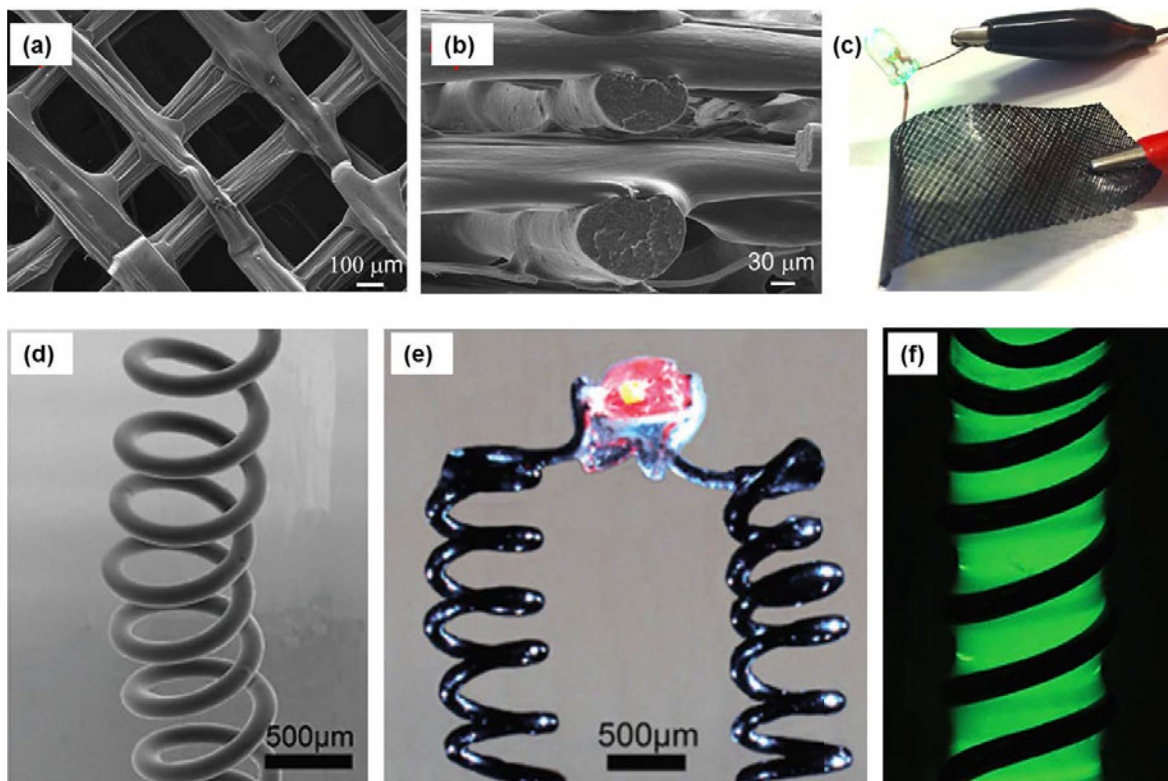
Fig. 19. 3D nanocomposite microstructures fabricated by the LDM and SC-3DP methods. (a) and (b) top-view and side-view SEM images of a MWCNTs/PLA nanocomposite scaffold fabricated by the LDM method and (c) photo of the scaffold turning on an LED light using a 3V CR2032-type watch battery, (d) SEM image of a freeform MWCNTs/PLA nanocomposite spiral fabricated by the SC-3DP method, (e) photo of two nanocomposite coils turning on an LED light when a DC current passes, and (f) optical image of a nanocomposite spiral used for liquid sensing in which a solvent was trapped inside the spiral upon the application of a low voltage.[12, 84]
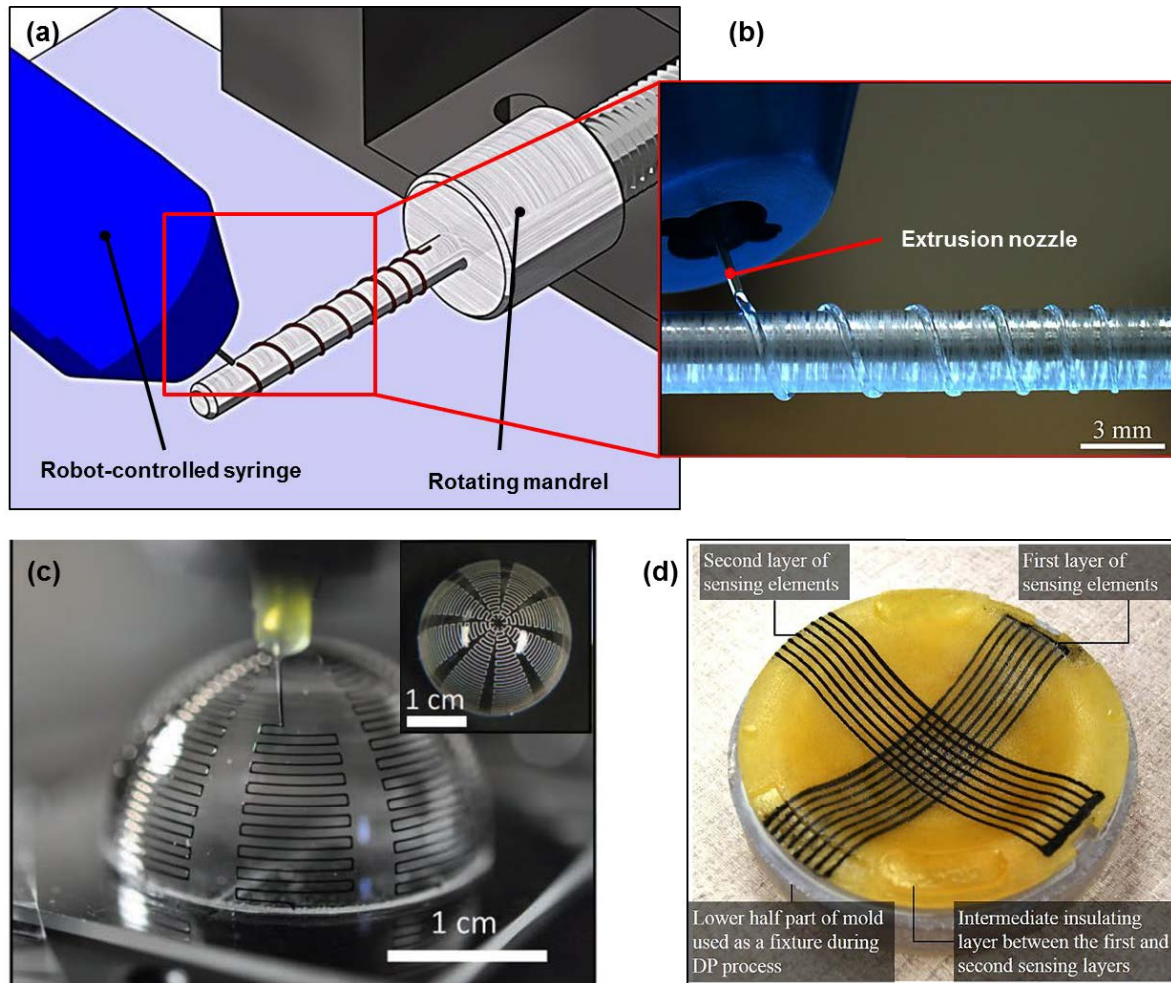
Fig. 20. Conformal 3DP technique: (a) and (b) schematic and optical representation of a conformal 3DP of a helical microcoil using a rotating mandrel,[71, 85] (c) optical images of small antennas printed onto a hemispherical glass substrate in the form of conductive meander lines (made of a silver nanoparticle ink),[11] and (d) optical image of a conformal 3D printed tactile sensor with two perpendicular sets of eight sensing elements using a MWCNTs-filled (0.5 wt.%) polymer nanocomposites.[87]
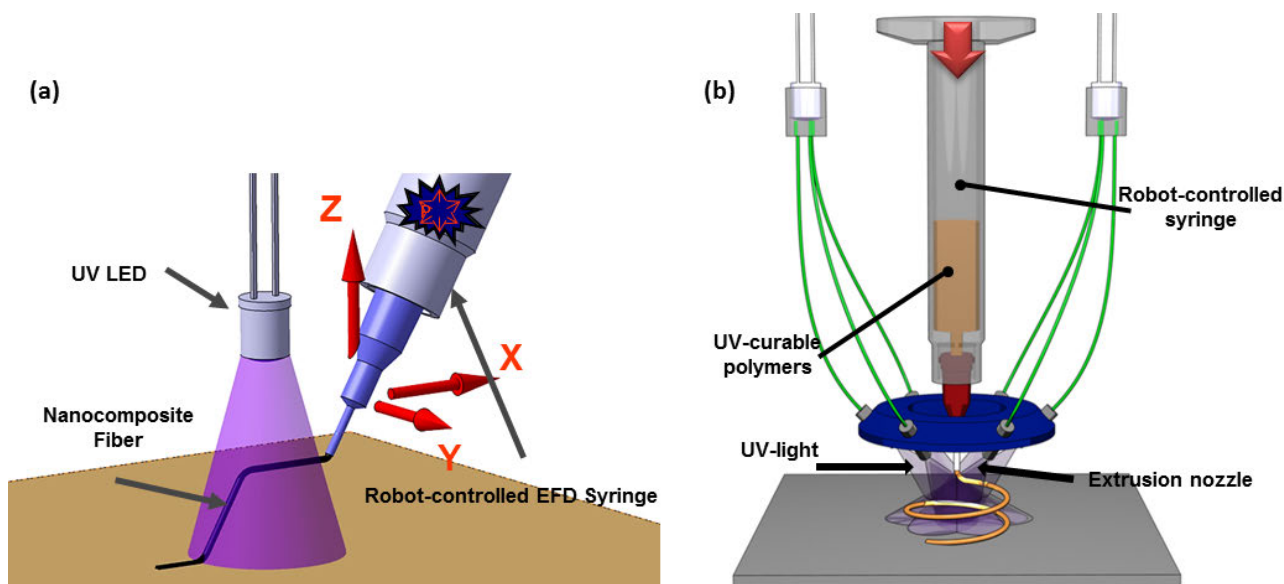
Fig. 21. Schematic illustration of the UV-3DP of (a) a freeform filament and (b) a freeform helical microstructure. The uncured viscos liquid material is photopolymerized within seconds after extrusion under UV exposure.[10, 70]
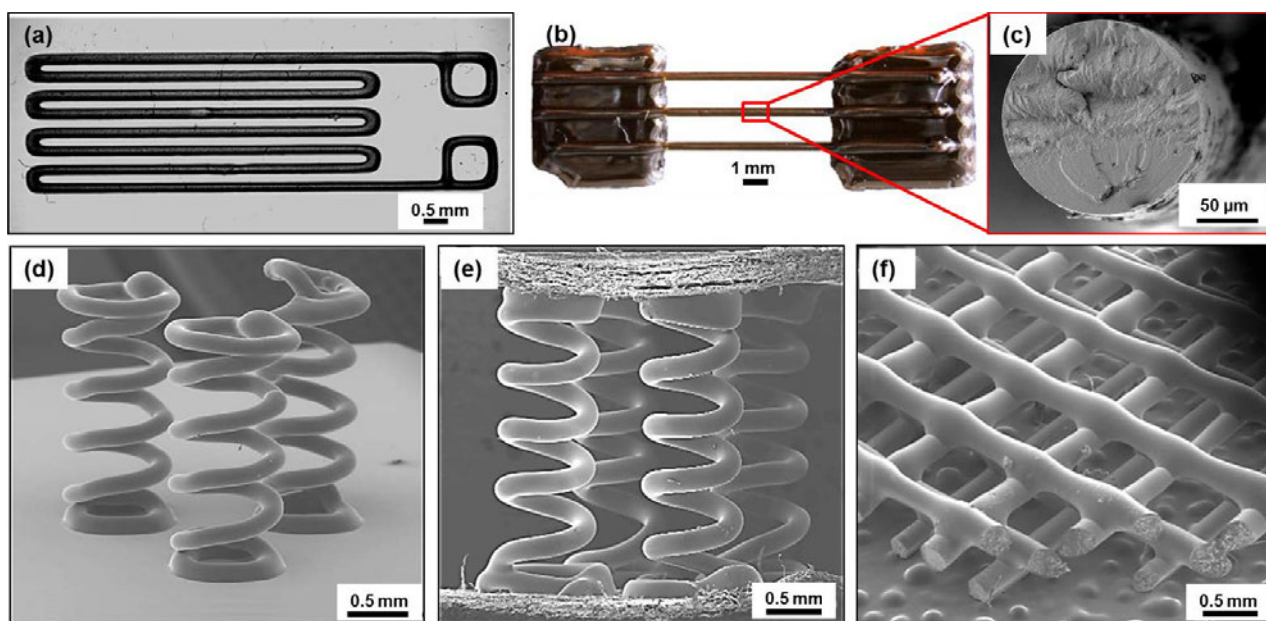
Fig. 22. Optical or SEM images of several carbon nanotube-filled nanocomposite microstructures fabricated using UV-3DP method. (a) a deposited 2D line network similar to traditional strain gauges (UV-epoxy/1 wt.% nanotubes), (b) a microfiber coupon composed of 3 fibers suspended between two nanocomposite tabs as a highly sensitive strain sensor (UV-epoxy/1 wt.% nanotubes) and (c) SEM image of fiber cross-section,[17] (d) SEM image of a triangular array of three helical nanocomposite (urethane-based/0.5 wt.% nanotubes) microcoils for load bearing MEMS components, (e) SEM image of a 3D nanocomposite (UV-epoxy/1 wt.% nanotubes) displacement sensor,[17] and (f) a four-layer nanocomposite (urethane-based/0.5 wt.% nanotubes) 3D periodic scaffold.[70]
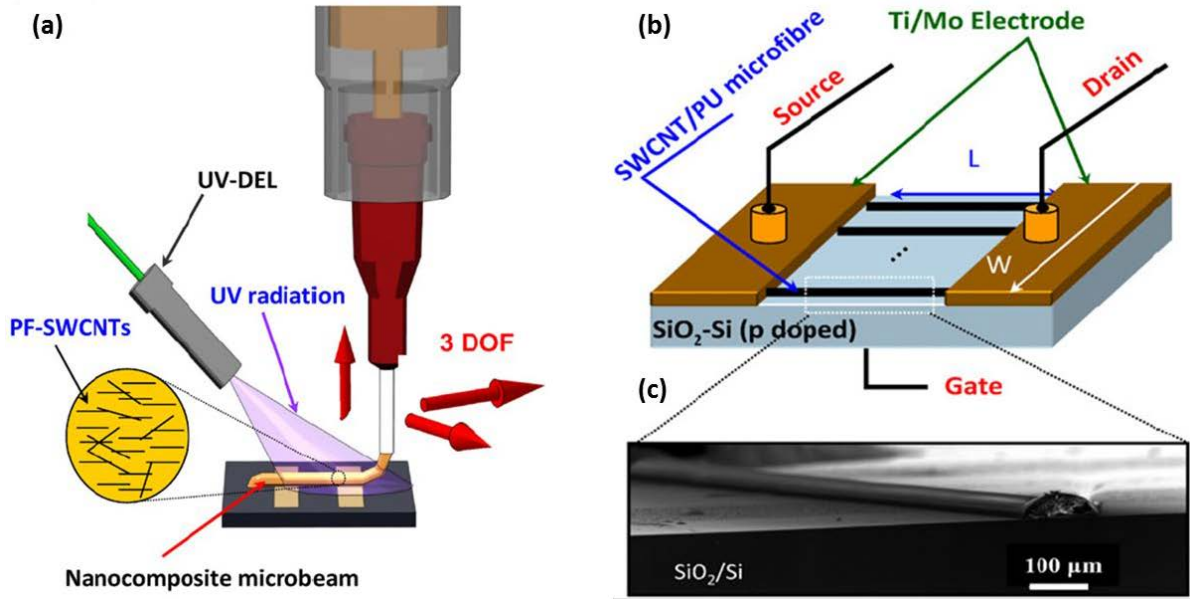
Fig. 23. Scheme of the UV-3DP of the nanocomposite microfilaments on a pre-patterned substrate, (b) the schematic representation of the FET device, and (c) optical image of a printed nanocomposite filament.[93]
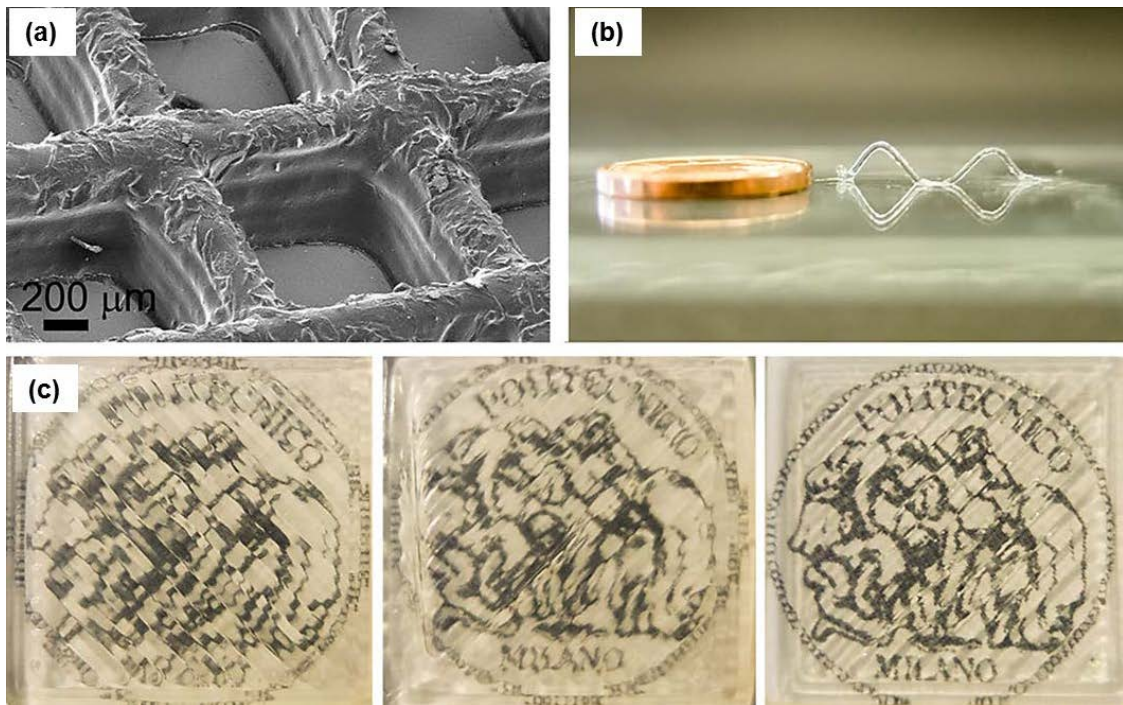
Fig. 24. UV-3D printed 3D and planar microstructures: (a) SEM image of a 6-layer matrix-like structure, (d) photo of a freeform spanning filament, and (c) optical photos of translucent planar structures of increasing transparency fabricated with different printing parameters.[94]
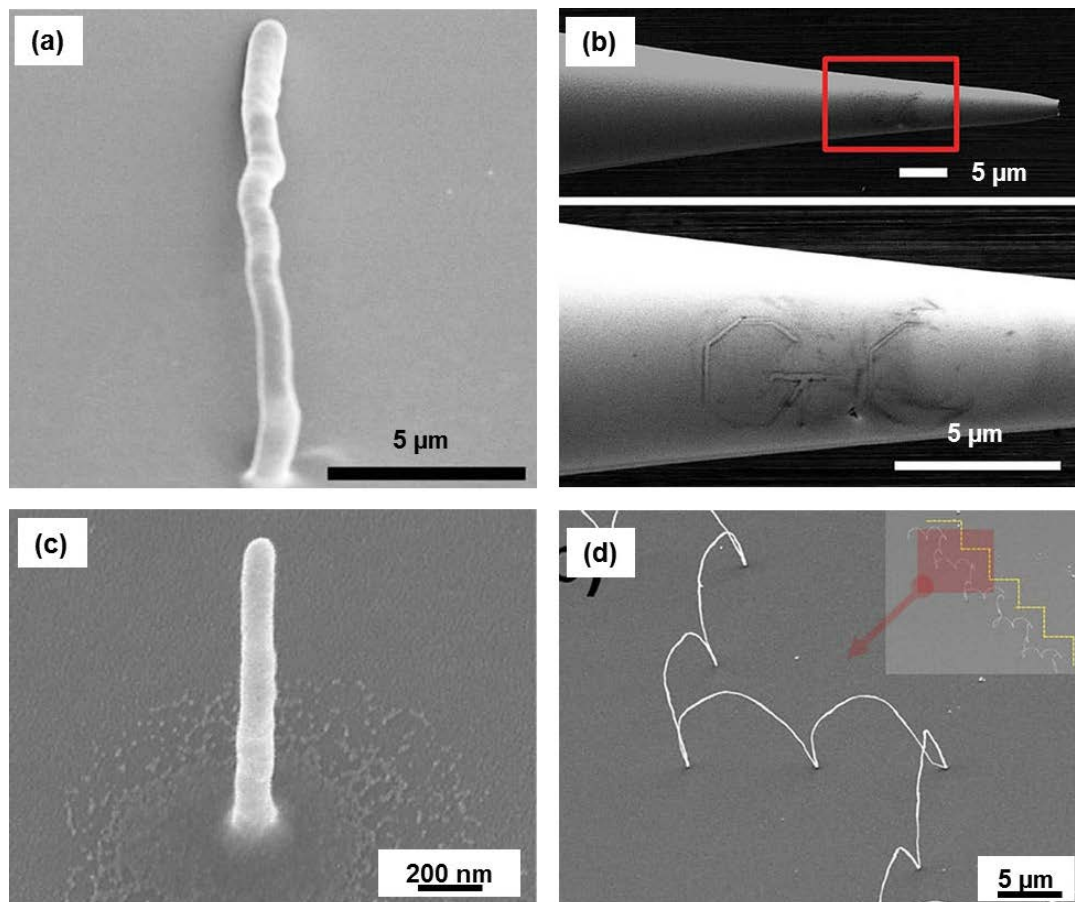
Fig. 25. SEM images of representative 3D printed structures using nanomaterial solutions: (a) an e-jet printed nanopillar fabricated using copper nanoparticle suspension (30 wt.%) mixed with n-tetradecane (1:1 weight ratio),[97] (b) rGO patterns e-jet printed on the sidewall of a glass microcapillary as a substrate fabricated using rGO nanoparticles dispersed in DMF. The capillary nozzle has a cone geometry with an internal diameter of 5 μm and a curvature radius of 50-65 μm,[95] (c) an e-jet printed gold nanopillar with diameter of ~50 nm and height of ~850 nm made of gold nanoparticle solution (~0.1 vol.% in a mixed solution of n-tetradecane and cyclododecene (50:1 wt./wt.)),[98] and (d) a zigzag rGO nanoarch with a constant arch width (r = 400 nm) fabricated via the meniscus-guided growth 3DP using an aqueous suspension of GO nanosheets,[99]

Table 1. Microfabrication techniques used for 3DP of nanocomposites.

Technique	Nanocomposite material used	Minimum feature size	Potential applications	Refs
Inkjet printing	Solution of photopolymers filled with silver and titanium nanoparticles, Annealed graphene sheets decorate with silver nanoparticles, Graphene hydrogel – polyaniline, Quantum dots filled photopolymers	Down to 60 μm	Strain gauge sensors, Flexible electronic devices, Nanocomposite supercapacitor, LEDs, sensing, data storage, anti-counterfeiting or visual indicators of increased temperature	[14, 52-54]
Powder bed technology	Carbon nanofiber/epoxy, Hydroxyapatite/graphene oxide nanoparticles,	Few hundreds microns	Load bearing bioapplications, optics, supercapacitors, water purification	[57, 58]
Microstereolithography (MSL)	Photopolymers filled TiO_2 nanoparticles	Few microns	Drag control in aircraft, beam focusing and steering, electromagnetic shielding and absorption	[63]
Dynamic optical projection stereolithography (DOPsL)	Hydrogel nanocomposites filled with polydiacetylene nanoparticles	Down to 2 μm	Detoxification for biomedical applications, flow sensor	[20, 66]
Direct-write assembly (DW)	Epoxy composite filled with clay nanoplatelets, nanocomposite conductive ink of silver nanoparticles, nanotube-filled epoxy, urethane or healing materials	Down to 2 μm	High performance composites, 3D photovoltaics, electronic and optoelectronic, light-emitting diodes, engineered microstructured nanocomposites, self-healing materials	[15, 31, 33, 73, 75]
Fused deposition modeling (FDM)	Thermoplastics (ABS or PLA) filled nanocrystalline hydroxyapatite or nanoclay	Down to 200 μm	Tissue engineering, noise reduction in earmuffs, electronic sensors	[80-83]
Solvent-cast 3DP (SC-3DP)	Thermoplastics (PLA) filled with nanotubes	Down to 80 μm	Liquid sensing, microelectronics	[9, 12, 84]
Conformal 3DP (C-3DP)	Nanocomposite conductive ink of silver nanoparticles, nanotubes filled photopolymers	Down to 100 μm	Microelectronics, antennas, multilayer tactile piezoelectric sensors	[11, 87]
UV-3DP	Photopolymers (urethane, epoxy) filled with nanotubes	Down to 100 μm	Field effect transistor, sensing applications, MEMS, microelectronics	[10, 17, 71, 93, 94]

Table 2. A summary of main process parameters, printing speed and cost for the 3DP techniques discussed in this review.

Technique	Main process parameters and their values used for 3DP of nanocomposites	Printing speed	Equipment cost	Refs
Inkjet printing	Voltage (e.g., 35V), frequency (e.g., 250-500 Hz), Nozzle diameter (e.g., 60 μm), its temperature (e.g., 40 °C), Drop spacing (e.g., 25-120 μm), viscosity (e.g., 0.02 Pa.s) Ink surface tension (e.g., 0.22 N/m)	Relatively slow	~$50000	[14, 52-54]
Powder bed technology	Adhesive-powder interaction, powder type, powder particle size (e.g., microns), adhesive droplet size (e.g., microns), viscosity (moderate)	Typically 2-4 layers per minute	0.05 – 2 M$	[57, 58]
Microstereolithography (MSL) / Two-photon polymerization	Laser intensity (e.g., 1.4 mW) Wavelength (e.g., 500-800 nm)	2 (mm/s)	a few thousand dollars	[63]
Dynamic optical projection stereolithography (DOPsL)	DMD device controls other parameters including light intensity at a single pixel level and material conversion rate	Very fast (e.g., 100 layers in ~10 seconds)	~$3000	[20, 66]
Direct-write assembly (DW)	Deposition speed (e.g., 0.1- 5 mm/s) Extrusion pressure (e.g., 0.5-1.4 MPa) Extrusion nozzle diameter (e.g., 0.5 -200 μm) Viscosity (moderate to high) and shear-thinning behavior (e.g., 100 Pa.s at low shear rates)	0.1- 5 mm/s	From $1000 for a simple home-made setup to >$15000 for dispensing robots	[15, 31, 33, 73, 75]
Fused deposition modeling (FDM)	Deposition speed (e.g., 0.1- 6 mm/s) Extrusion pressure (e.g., 1.4-2 MPa) Extrusion nozzle diameter (e.g., 200-500 μm) Temperature (depending on polymer melting point) Viscosity (depending on viscosity at melting point)	0.1- 6 mm/s	$200 - $330000	[80-83]
Solvent-cast 3D printing (SC-3DP)	Solvent/nanocomposite proportion (e.g., 70/30 wt./wt.) Deposition speed (e.g., 0.1- 5 mm/s) Extrusion pressure (e.g., 1.4-2.5 MPa) Extrusion nozzle diameter (e.g., 10-300 μm)	0.1- 5 mm/s	$1000 - $15000	[9, 12, 84]
Conformal 3D printing (C-3DP)	Deposition speed of (e.g., 0.1- 10 mm/s) Extrusion pressure (e.g., 0.7-2.5 MPa) Extrusion nozzle diameter (e.g., 30-535 μm)	0.1 – 10 mm/s	$1000 - $15000	[11, 87]
UV-3D printing (UV-3DP)	Deposition speed (e.g., 0.1-30 mm/s) Extrusion pressure (e.g., 1.4-2.8 MPa) Extrusion nozzle diameter (e.g., 100-1500 μm) UV radiation intensity (e.g., 50 mW cm^{-2}) Viscosity (e.g., 100-400 Pa.s at low shear rates)	0.1-30 mm/s	$1500 - $15000	[10, 17, 71, 93, 94]

About the authors:

Dr. Rouhollah D. Farahani is a postdoctoral researcher, holding the prestigious NSERC award in the department of Mechanical Engineering at Ecole de technologie supérieure, Montreal, Canada. Rouhollah completed his Ph.D. in 2012 at Polytechnique of Montreal working on 3D printing of epoxy-based nanocomposites. His expertise is related the design of advanced nanocomposite materials for the manufacturing of multifunctional microsystems and engineered materials with optimized properties using innovative cost-effective manufacturing techniques. He has contributed to several articles in high impact factor journals (*e.g., Nanoscale, Nanotechnology, Langmuir*) in the fields of 3D printing and nanotechnology.

Prof. Daniel Therriault is a professor in the department of Mechanical Engineering at Polytechnique of Montreal, Canada. He is also Canada Research Chair in Fabricating Microsystems and Advanced Materials. His expertise is related to the design and characterization of advanced materials for the manufacturing of 3D multifunctional microsystems. He is the principal investigator of several innovations including a breakthrough 3D freeform printing method called UV-assisted 3D printing (*Advanced Materials, 2010)*. He has contributed to several articles in high impact factor journals (*e.g., Nature Materials, Advanced Materials, Small, Nanoscale*) in the field of 3D printing of advanced materials.
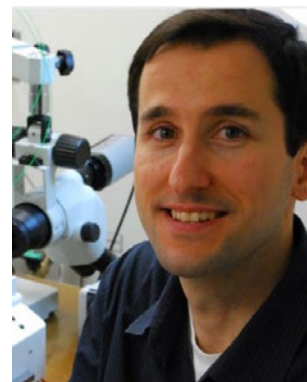
Prof. Martine Dubé is a professor in the department of Mechanical Engineering at Ecole de technologie supérieure, Montreal, Canada. Her research interests mainly focus on joining of thermoplastic composite materials by welding, repair of composite structures and processing of thermoplastic composites. Prof. Dubé is involved in a large-collaborative project on the development of new heating element types based on nanomaterials and nanocomposites for resistance and induction welding of thermoplastic composites for aerospace applications.

Table of contents entry:

The purpose of this paper is to review the literature related to different three-dimensional (3D) printing techniques used to fabricate 3D structures made of nanocomposite materials. Various examples of 3D macro- and microstructures manufactured using different 3D-printing technologies for a wide range of domains such as MEMS, lab-on-a-chip, microfluidics, engineered materials and composites, microelectronics, tissue engineering and biosystems are reviewed.
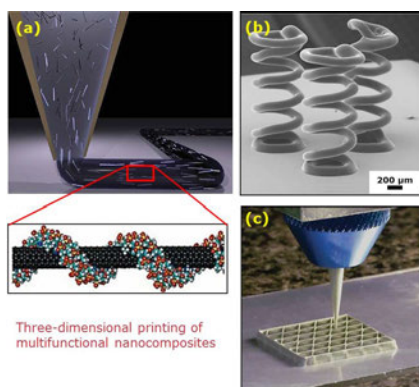
Fig. ToC. 3D printing of multifunctional nanocomposites and representative applications: (a) schematic illustration of 3D printing of nanocomposites, (b) SEM image of a triangular array of three helical nanocomposite microcoils for load bearing MEMS components and sensors, and (c) optical image of a 3D printed high-performance cellular composite.

Prof. M. D. Author-Two, Prof. D.T. Author-Three, Dr. R. D. F Corresponding-Author

Supplementary online information

Table S1. Additional information regarding the suppliers/manufacturers of the main equipment used in the 3DP techniques mentioned in this review.

Technique	Suppliers of main equipment used
Inkjet printing	http://microfab.com/complete-systems http://www.fujifilm.ca/press/news/display_news?newsID=880143 http://proto3000.com/polyjet-3d-printing-services-rapid-prototyping.php
Powder bed technology	http://www.3dsystems.com/ http://www.zcorp.com/documents/108_3D%20Printing%20White%20Paper%20FINAL.pdf
Microstereolithography (MSL)	https://www.aerotechgmbh.de http://www.zeiss.com/microscopy/en_de/home.html
Dynamic optical projection stereolithography (DOPsL)	http://www.aerotech.co.uk/product-catalog/stages.aspx http://www.ti.com/product/dlp7000 http://www.projectorcentral.com/Compaq-MP1800.htm
Direct-write assembly (DW)	http://www.aerotech.com/product-catalog/stages.aspx http://www.nordson.com/en/divisions/efd/products/fluid-dispensing-systems/ultimus-v-high-precision-dispenser http://www.fisnar.com/products/desktop-robots http://www.nordson.com/en/divisions/efd/products/fluid-dispensing-systems
Fused deposition modeling (FDM)	http://www.solidoodle.com/ https://www.lpfrg.com/ http://www.fisnar.com/products/desktop-robots http://www.nordson.com/en/divisions/efd/products/fluid-dispensing-systems/hpx-high-pressure-dispensing-tool
Solvent-cast 3D printing (SC-3DP)	http://www.fisnar.com/products/desktop-robots https://www.futurashop.it/3drag-stampante-3d-versione-1.2-in-kit-7350-3dragk http://www.nordson.com/en/divisions/efd/products/fluid-dispensing-systems/hpx-high-pressure-dispensing-tool
Conformal 3D printing (C-3DP)	http://www.micosusa.com/old/Con_5018.html http://www.aerotech.com/product-catalog/stages/linear-x-y-stages/abl9000.aspx http://www.sutter.com/MICROPIPETTE/p-2000.html http://www.gpd-global.com/co_website/pcdpumpseries-pcdmodels.php
UV-3D printing (UV-3DP)	http://www.fisnar.com/products/desktop-robots http://www.nichia.co.jp/en/product/uvled.html http://www.nordson.com/en/divisions/efd/products/fluid-dispensing-systems/hpx-high-pressure-dispensing-tool